Study of Adsorption-based Technology for Removal/Detection of Trace Inorganic Contaminants in Water

July 2018

Li Jie

Study of Adsorption-based Technology for Removal/Detection of Trace Inorganic Contaminants in Water

A Dissertation Submitted to

the Graduate School of Life and Environmental Sciences,

University of Tsukuba

in Partial Fulfillment of the Requirements

for the Degree of Doctor of Philosophy in Environmental Studies

(Doctoral Program in Sustainable Environmental Studies)

Li Jie

Abstract

In the past decades, deterioration of the water environment has frequently occurred owing to uncontrolled anthropogenic activities. Meanwhile, the rapid industrialization and urbanization processes demand more qualified water for domestic, agricultural, and industrial purposes. More than ever before, the existing source freshwaters need effective purification to ensure the drinking water quality, and wastewaters must be sufficiently and effectively treated to minimize their disturbances on the natural water bodies. In a word, the need for technological innovations to enable effective water and wastewater treatment cannot be overstated.

As for the trace inorganic contaminants, especially those with high toxicity and low biodegradability (like arsenic, copper, and cyanide, etc.), the porous materials based adsorption technology has been extensively studied for target pollutants' sensing and removal. However, up to now, the industrial-scale application, or their scaling up application from laboratory research to the real world is still lacking. One major cause is the discrepancy between the ideal conditions in theory and the real water environment in practice, which gives birth to the overstated effect of many newly reported materials. Another concern comes from the powdery shape, the main existing form of most porous materials but with a great deal of inconvenience in practical application.

In this study, efforts were made to obtain novel porous materials which are more realistic to the practical application: (1) one kind of novel porous material (Zeolitic imidazolate frameworks-8, ZIF-8) was synthesized and applied for the removal of arsenate, especially for trace (ppb, $\mu g/L$) arsenate removal in a more realistic water environment; (2) silk fiber was applied as the substrate for the deposition of a typical fluorescent porous material (Metal-organic framework-76(Tb), MOF-76(Tb)), so as to realize the easy separation and prevent the loss of the powdered material during its further usage in copper detection; and (3) powdered activated carbon was modified with polyamidoamine (PAMAM) for surface functionality and used as disposable material for cyanide removal. Major results are summarized as below.

(1) ZIF-8 was explored for the removal of trace arsenate from water. Results showed that

ZIF-8 outperformed some other adsorbents, achieving the first and highest reported adsorption capacity (76.5 mg/g) at a low equilibrium concentration (9.8 μg/L). Satisfactory adsorption properties (adsorption capacity, adsorption rate, adaptability to water environment, regeneration capacity) demonstrated the feasibility of using ZIF-8 as an efficient adsorbent for the removal of aquatic trace arsenate. In addition, fourier transform infrared (FTIR) and X-ray photoelectron spectroscopy (XPS) spectra revealed the proposed mechanism of As(V) adsorption onto ZIF-8 which can create large amounts of external active sites (Zn-OH) through the dissociative adsorption of water, subsequently forming an inner-sphere complex with arsenate molecules. Insights into the adsorption process uncovered the key factors to the formation of this high removal efficiency: the hydration process to form surface hydrogen group by dissociative adsorption of water, the high accessible surface area, and the cooperative interaction (e.g., Van der Waals' force and hydrogen bonding) between As(V) species at a low surface coverage.

(2) Domestic silk fiber was utilized as the skeleton for the coating of dense luminescent MOF-76(Tb) layers. Its surface functionality consisting of abundant intrinsic carboxylic groups, smooth surface structure, and 80% of tensile strength was maintained after being immersed in different thermal solvents (water, ethanol, DMF @ 80°C) for 24 h, revealing its good solvent and thermal resistance. By using hydrothermal, microwave assisted, and layer-by-layer methods, different crystal morphologies (pillar-like, sedimentary-rock-like, and needle-like morphology) and varying degrees of surface coverage rate were obtained, attributable to the different levels of anchoring promotion and crystal controlling effect. The MOFs coating was confirmed by its XRD pattern and fluorescent property. More importantly, the quenching effect of the composite in a condition of Cu^{2+} was first reported with high selectivity, sensitivity (i.e. a linear detection concentration range of $10^{-3} \sim 10^{-5}$ M with a low detection limit up to 0.5 mg/L, K_{SV} of 1192 M^{-1} at 293 K), and rapid response time (5 min), making the composite a good candidate for colorimetric and fluorescent detection of aquatic Cu^{2+}. The quenching mechanism is proposed to be associated with the interaction between Cu^{2+} and benzene-tricarboxylate (BTC) ligand, which leads to the decrease of energy transfer efficiency. The selectivity over other

common cations depends on the unsaturated electron configuration and the smaller ionic radius of Cu^{2+}.

(3) A novel integrated process of coagulation and adsorption was also proposed in this study for the advanced treatment of biologically pretreated coking wastewater. Results from the laboratory, pilot, and industrial-scale experiments indicate that this one-step novel process can remove bio-refractory pollutants, achieving the maximum chemical oxygen demand (COD) and cyanide removals of around 85.3% and 99.4%, respectively. Its effluent could meet the corresponding discharge standards without any further treatment, i.e., COD < 30 mg/L, cyanide < 0.1 mg/L, and improved effluent safety (lower toxicity). The easy operation and high efficiency of this method reflect its great potential for engineering application in the tertiary treatment of coking wastewater.

Results from this work are expected to provide new concepts and useful information for the application of porous materials based adsorption technology in the real practice of water/wastewater treatment and water quality monitoring.

Contents

List of tables

List of figures

Acronyms and abbreviations

AC:	Activated carbon
ALD:	Atomic layer deposition
COD:	Chemical oxygen demand
DMF:	N,N-dimethylformamide
EDS:	Energy dispersion spectrum
FTIR:	Fourier transform infrared
HT:	Hydrothermal method
LBL:	Layer by layer method
MF:	Microfiltration
MOFs:	Metal-organic frameworks
MPAC:	Modified powdered activated carbon
MWA:	Microwave assisted method
NF:	Nanofiltration
ORP:	Oxidation-reduction potential
PAC:	Poly-aluminum chloride
PAM:	Polyacrylamide
PAMAM:	Polyamidoamine
PFS:	Poly ferric sulfate
RO:	Reverse osmosis
SAMs:	Self-assembled monolayers
SEM:	Scanning electron microscope
TEM:	Transmission electron microscope
UF:	Ultrafiltration
XRD:	X-ray diffraction
XPS:	X-ray photoelectron spectroscopy
ZIF-8:	Zeolitic Imidazolate Framework-8

Chapter 1 Introduction

Water is the most precious resource and essential substance for human civilization and all life on Earth. Unfortunately, due to the situation of water resource deficiency and water environment deterioration, safe drinking water supply has become a major global challenge in the 21st century. On one hand, the improvement of living standard demands for increasingly stringent water quality; On the other hand, the water environment has been seriously polluted by uncontrolled anthropogenic activities. Thus, the effective treatment of drinking water and wastewater is essential for keeping the social cycle of water resources and resolving the water crisis.

1.1 The situation of water shortage and water contamination worldwide

In the 20th century, the world population quadrupled while the global water demand increased sevenfold [1]. In the coming decades, the growing industrialization and urbanization process will continue to intensify the water demand from domestic, agriculture, and industry perspectives [2]. During 1995 and 2025, it is estimated that the areas affected by "severe water stress" expand and increase from 36.4 to 38.6 million km^2; The number of people living in these areas also increases from 2.1 to 4.0 billion; And there will be even tension between nations because of strong competition for the scarce water resources [3, 4].

In addition to overall water shortage, poor water quality is near crisis in many parts of the world. Until 2015, only about 20% of the global wastewater has been properly treated. In developing countries, nearly 70 percent of the industrial wastewater is discharged directly without proper treatment [5]. Widespread organic pollution, toxic pollution, and eutrophication were caused by the random emission of various pollutants. Taking China as an example, according to the China Environmental State Bulletin published by Chinese Ministry of Environmental Protection (2016), 26.8% of the 1940 river monitoring sections are at a water quality of grade IV or worse, of which the source water is not suitable for being used as drinking water [6]. Moreover, the water quality in 8.6% sections is below grade V, the worst grade in the Chinese national standard for water quality, and this kind of water resource is virtually of

no functional use. For Haihe River, which supplied Beijing city with the bulk of raw water before, this percentage was even as high as 41.0%.

Water on the Earth is under constant motion between the great natural cycle and small social cycle. Between them, the social cycle is the unity of urban water supply and drainage. More than ever, the existing fresh water resources need effective treatment to ensure the drinking water quality, and the wastewater must be given sufficient treatment to minimize the disturbance of social water cycle on natural water cycle. In a word, the need for technological innovation to enable effective water and wastewater treatment cannot be overstated [7].

1.2 Inorganic contaminants and their sources

The water pollutants can be categorized into three main types: inorganic, organic, and biological ones in nature. For inorganic contaminants, there are two main sources in natural water: (1) the anthropogenic activities, especially mining and smelting industries, from which large amounts of effluent and pollutants are discharged into the surface water bodies; (2) the natural geochemical processes, through which the nature chemicals are leached into the groundwater by rock water interaction [7, 8].

1.2.1 Surface water contamination from anthropogenic activities

Mining and the subsequent processing activities are the extraction of miners and valuable resources (metals, coal, and diamonds, etc.) from the Earth's crust. The mining and smelting industries have played an important role in the development of modern human civilization. At the same time, a significant environmental expense should be recognized that the mining and minerals processing activities have seriously negative impact on the water environment [9, 10].

The extraction of miners produces up to one thousand tons of wasted material for per kg of pure material [11]. It is estimated that more than 50 billion metric tons of geological waste was mobilized by mining activities each year, which is equal to the amount of particles transported by river from the continent [12]. Serious water environment contamination was caused because of large waste deposits, exposed to oxidation condition by air and weathering by precipitation, and then the pollution of water bodies [13]. Consequently, the contamination of water environment by inorganic pollutants is unavoidable under long-time exposure to heavy

metals, which are originally sequestered inside the Earth's crust as ore deposits [9].

Additionally, extraction of precious resources (lignite, copper, and gold, etc.) from ores consumes and then discharges large amount of chemicals that pose greater pollution hazards and risks to the environment. Taking the gold production as an illustrative example, typically, 140 kg of cyanide chemicals are consumed to extract 1 kg of gold, which would be dispersed into the environment in the form of deposit or wastewater subsequently [11]. For the coal production, the effluent containing greater than 100 mg/L of cyanide is produced during the coking process [14].

1.2.2 Groundwater contamination from geogenic processes

In addition to the anthropogenic activities, the geological process, in some areas of the world, is another source leaching chemicals into water bodies. The main concern includes arsenic, fluoride, uranium, etc. [15]. At the global scale, natural processes are predominantly responsible for the elevated concentrations of fluoride and arsenic [16, 17]. For the large scale arsenic release, two 'triggers' are concluded: strongly reducing or alkaline conditions (with pH > 8.5) in semi-arid or arid environments, which lead to dissolution of arsenic containing minerals or the desorption of adsorbed arsenic species, respectively [16, 18]. As a result, the arsenic species is quite soluble and mobile, and rich in the aquatic environment, especially in groundwater.

1.3 Typical kinds of highly toxic inorganic pollutants

1.3.1 Arsenic contamination

Among all the geogenic contaminants, arsenic has significantly negative impact on human health, and caused a global concern as well. For this reason, arsenic is taken as an illustrative example. Arsenic (As) is a metalloid element that exhibits excessive levels of toxicity. Prolonged exposure to an arsenic-contaminated environment could cause chronic and acute toxicity, cancer, and even death [19]. Unfortunately, arsenic pollution in groundwater and surface water has frequently occurred in the past decades because of the geochemical processes and uncontrolled anthropogenic activities. According to the statistics, a total of 105 countries

and up to 226 million people worldwide are suffering from arsenic pollution [20]. In China alone, there are 19.6 million people affected by arsenic contaminated drinking water [21]. Given the absence of effective therapeutic measures for arsenic toxicity, the key prevention measure is to avoid exposure to arsenic sources and ensure the arsenic concentration in drinking water below the safety limit (10 μg/L). Thus, studies have focused on the removal of aquatic As(V) [22].

1.3.2 Heavy metals contamination

The most common inorganic pollutants are heavy metals which are toxic and carcinogenic in nature [23]. The term of "heavy metal" is generally applied to the group of elements with atomic density greater than 6000 kg/m^3 [24], like copper (Cu), cadmium (Cd), chromium (Cr), lead (Pb), and mercury (Hg), which are natural components of the Earth's crust [25] and are introduced to the water environment as a result of growth of mining and smelting industry. Being different from other heavy metals, copper is an essential micronutrient for living beings because of its role in enzyme synthesis, bones and tissues development [24]. However, excessive copper consumption can lead to liver and kidney failure [24]. Thus, reliable sensing and removal of copper ions are crucial for water environment protection for human beings.

1.3.3 Cyanide contamination

By the late 1990s, the usage of cyanide to extract gold from ores had been widely applied and supported more than 90% of the global gold production [26]. As a result, accidental spills of cyanide containing wastewater often happened, which was usually taken as the most significant cyanide releases into the water environment [26]. Another main cause comes from the coal processing sites (coking industry) where cyanide is not sufficiently removed or detoxified. Predictably the serious cyanide contamination will continue for a long time because of our dependence on the related mining industry.

The cyanide added to the extraction process is in the form of cyanide anion, and the product leached from the coal and gold ore includes several other cyanide-containing and cyanide-related species, like free cyanide (CN$^-$, HCN), cyanate (CNO$^-$), thiocyanate (SCN$^-$), and cyanometallic complexes [27], which pose a high risk to aquatic organisms and aquatic-

dependent organisms in the environment.

1.4 Current technologies for mitigation of aqueous inorganic pollutants

Facing the steadily rising demand for clean water, there is an increasing need for efficient strategies to mitigate water contamination. Although many new methods have been employed for the treatment of inorganic contaminants, the practical methods are still limited to the main techniques listed as follows.

1.4.1 Chemical precipitation

Chemical precipitation is an effective and simple way to treat the inorganic contaminants. In precipitation processes, chemicals are added to react with the target contaminants and form insoluble precipitates. And the removal of pollutants is realized through the separation of solid waste from the liquid. The conventional chemical precipitation processes include hydroxide precipitation for copper removal, lime precipitation for arsenic removal, and metal precipitation for cyanide removal.

Chemical precipitation has been widely used in the past because of its simplicity and inexpensive treatment cost. However, this method is usually applied for treating high concentration pollutants, which is ineffective when treating trace pollutants like arsenic in the groundwater. Furthermore, the chemical precipitation method produces a large amount of sludge and causes secondary pollution, leading to its limited application.

1.4.2 Coagulation-flocculation

Coagulation and flocculation followed by sedimentation process is widely used for the treatment of both drinking water and wastewater.

Coagulation is the process of destabilizing the colloid particles by compression of electric double layer and charge neutralization process. In addition to the conventional coagulants such as aluminum salt, ferrous sulfate, and ferric chloride, many novel chemicals have been developed, including poly-aluminum chloride (PAC) and poly-ferric sulfate (PFS). As it is known, the pre-hydrolyzed aluminum coagulant, i.e. PAC contains much more active species (Al_{13} or Al_b, $AlO_4Al_{12}(OH)_{24}^{7+}$), thus exhibiting enhanced coagulation efficiency due to its

strong adsorption and bridging capacities in addition to higher positive charges [28, 29].

Flocculation is the process of the destabilized particles to bind other particles and form large agglomerates or clumps (flocs), which is easier to be removed in the subsequent sedimentation or filtration process. Polyacrylamide (PAM) is a typical flocculant with widespread usage. Those colloidal particles are removed by the enmeshment of the impurities on the formed amorphous precipitates.

Although coagulation-flocculation method has long been known to be effective for water treatment, it has been found that this process can't treat the water or wastewater completely, especially for trace and soluble contaminants [30-32]. Therefore, coagulation-flocculation process must be coupled with other treatment techniques, so as to ensure sufficient removal of the pollutants.

1.4.3 Membrane filtration technology

Membrane filtration processes are pressure driven separation processes, where the driving force is the pressure difference across the membrane [33]. The membrane allows the purified fluid to pass through it while rejecting the contaminants: the feed water to be treated is separated into a stream of permeate and a remaining quantity of retentate, also known as concentrate [34]. Because of its high efficiency, easy operation and space saving, membrane processes including microfiltration (MF), ultrafiltration (UF), nanofiltration (NF) and reverse osmosis (RO) have become important treatment units for water purification.

Despite being taken as the 21st century water treatment technology, the inherent problems such as process complexity, high cost, membrane fouling and falling permeate flux limit its wide application in wastewater treatment, especially in developing countries with limited economic and management capacity.

1.4.4 Adsorption technology

Adsorption is a process of liquid solute accumulating on the surface of a solid material (adsorbent), and forming a molecular or atomic film (the adsorbate) [35]. Because of its simplicity and cost effectiveness, adsorption is currently considered to be very suitable for water and wastewater treatment and has been used for purification of various effluents [36, 37]. The

key to adsorption technology is the development of highly efficient adsorbents. The commonly used adsorbents include activated carbons, natural mineral materials (like zeolite), bio-adsorbents, and some newly developed novel materials like nano-adsorbents.

1.5 Porous adsorbent materials

1.5.1 Activated carbon

Of the various adsorbents available for the removal of pollutants, activated carbon (AC) has been taken as the most widely used material for the removal of trace contaminants in water and wastewater treatment. It is a highly porous and amorphous solid material, consisting of micro crystallites with a graphite lattice and usually prepared in granular or powder shape [35].

The AC material is originally applied for the adsorption of organic pollutants and nonpolar substances due to its hydrophobic property. For inorganic contaminants removal, the modification of carbon surface (chemical property) is essential, which has been recognized as a promising way for new applications of conventional carbon material in many fields [38]. Modification of AC involves acidic and base treatment, impregnation, ozone treatment, microwave treatment, plasma treatment, biological modification, etc. Various functional groups (e.g., amine, carboxylic acid, etc.) could be introduced to the AC surface by using the above mentioned modification methods.

For arsenic removal, iron salts have been widely used for preparation of AC impregnation. Huang and Vane modified the activated carbon with iron salt for arsenate removal, and a 10-fold adsorption capacity was achieved when compared with the untreated AC material [39]. The mechanism concerned involves the formation of iron-arsenate complexes [40-43]. In addition to a higher adsorption capacity, the adsorption rate of Fe^{3+} impregnated granular activated carbon (GAC-Fe) was faster than the untreated GAC, even in presence of dissolved Fe^{2+}, Fe^{3+}, and Mn^{2+} [44].

For copper adsorption, various methods have been applied for the enhancement of adsorption capacity. Strelko and Malik modified the commercial activated carbon using nitric acid to introduce a variety of surface carboxylic groups, which can function as the dominant group to anchor copper ions [45]. With the impregnation strategy, Yang et al. prepared Fe-

impregnated activated carbon (Fe-AC) and assigned the additional copper removal capacity to the surface complexation reaction between copper and surface Fe(III) species [46].

For cyanide removal, Adhoum and Monser found that carbon-Ag impregnation composite had cyanide removal capacity of nearly two times that of carbon–Ni impregnation and of four times that of plain activated carbon [47].

1.5.2 Novel porous nano-adsorbents

Recently, there has been an emphasis on the development of novel nano-adsorbents that can function as efficient and viable alternatives to AC. Typical materials include nanoparticles, carbonaceous nanomaterials, silicon nanomaterials, nanofibers, nanoclays, polymer-based nanomaterials, xerogels and aerogels, etc. [48]. Among these mentioned materials, Metal-organic frameworks (MOFs, one kind of coordination polymers) are superior to other porous materials because of high chemical and thermal stability, large accessible surface area, and abundant active surface sites [49].

MOFs are basically composed of two major components: a metal ion or a cluster of metal ions and an organic molecule called a linker [50], which are linked through self-assembly processes. Recently, MOFs have been widely investigated for the adsorptive removal of hazardous materials through additional interaction between adsorbates and the active sites of MOFs, such as central metals, unsaturated sites, functional linkers, and loaded active species, etc. [49]. These properties confer the material with great application potential and make them promising candidates in adsorption.

1.6 The state of the art of porous adsorbents development and application

In the past few years, an enormous amount of research effort went into the adsorption technology and the development of novel porous materials for water treatment. However, upon reviewing the industrial-scale treatment processes, the long time's delay from laboratory-scale demonstration and obvious efficiency reduction in industrial process is striking. Two main factors are associated with this gap between the laboratory and industrial performance as addressed below.

1.6.1 Discrepancy of removal efficiency between the ideal conditions and the real practice

The obvious efficiency reduction from the laboratory demonstration to application is a great challenge for the industrialization of adsorption technology. The sharp difference between the ideal conditions and real water environment is the major cause for this efficiency gap. For example, many reported works obtained the maximum capacity from the Freundlich or Langmuir models, which provides a very limited reference value since the strict model precondition usually can't be realized in the real practice. In some extreme cases, in order to obtain higher capacity value, a particular high initial concentration was employed to give enough concentration gradient, which is not in accordance with the actual concentration range of the pollutants in the environment. As a result, the subsequent application usually has serious discrepancies with the result obtained from the laboratory test. In addition, various factors including the co-existing ions, basic or acidic environment, and temperature may, to a great extent, have impact on the actual performance of the adsorbent materials. To conclude, there is a pressing need for objective evaluation of the newly-developed adsorbent materials and reliable experimental data for their further large-scale applications, which focus on the inorganic contamination control in practice instead of obtaining the maximum capacity in theory.

1.6.2 Inconvenience nature of powdered materials in practice

Another challenge comes from the powdery shape, which is the main existing form of most porous materials but with a great deal of inconvenience in practical usage. During the static adsorption process, the separation of solid from aquatic system is quite difficult, especially for those fine particles like nano-adsorbents. For the dynamic adsorption mode, continuing head pressure is needed because of the huge flow resistance caused by the filler. To solve the problem of its inconvenient usage, the deposition of powdered material onto other substrate is essential and has been recognized as one of the most critical issues. An alternative method is to develop disposable adsorbent by taking not only the functions for water treatment, but also the feasibility and cost-effectiveness into consideration.

1.7 Research objectives and thesis structure

Contrary to other techniques that are usually energy intensive and complex in operation, adsorption technology is easy and cost-effective. So, it is logical to investigate the means to further improve the efficiency of the adsorption technology in water treatment or quality monitoring. The objective of this study was to better identify and mitigate the inorganic contamination (arsenate, copper and cyanide) in water by adopting a more pragmatic approach. Given the poor performance of the reported porous material when treating real water samples, a more realistic water environment and the real coking wastewater sample were applied for the investigation of trace arsenate (ppb, μg/L) and cyanide removal, respectively. To overcome the inconvenience of powdered materials in solid-liquid separation, the feasibility of coating porous material onto other substrate and preparing the disposable material were explored for the copper ions detection and cyanide containing wastewater (coking wastewater) treatment, respectively. The framework of the thesis structure is displayed in Fig. 1-1.

The main contents of this thesis include five parts. In chapter 1, the research background, significance, literature review and the thesis framework were given. In chapter 2, a special attention was paid to the adsorption removal of arsenate from raw water, especially for trace (ppb, μg/L) arsenate in a more realistic water environment. In chapter 3, the feasibility of depositing powdered porous material onto the domestic silk fiber was investigated, in order to realize feasible copper detection in the practice of water quality monitoring. In chapter 4, the feasibility of preparing a disposable composite material was focused for the advanced treatment of coking wastewater (cyanide removal). In chapter 5, conclusions were summarized with the future research being prospected.
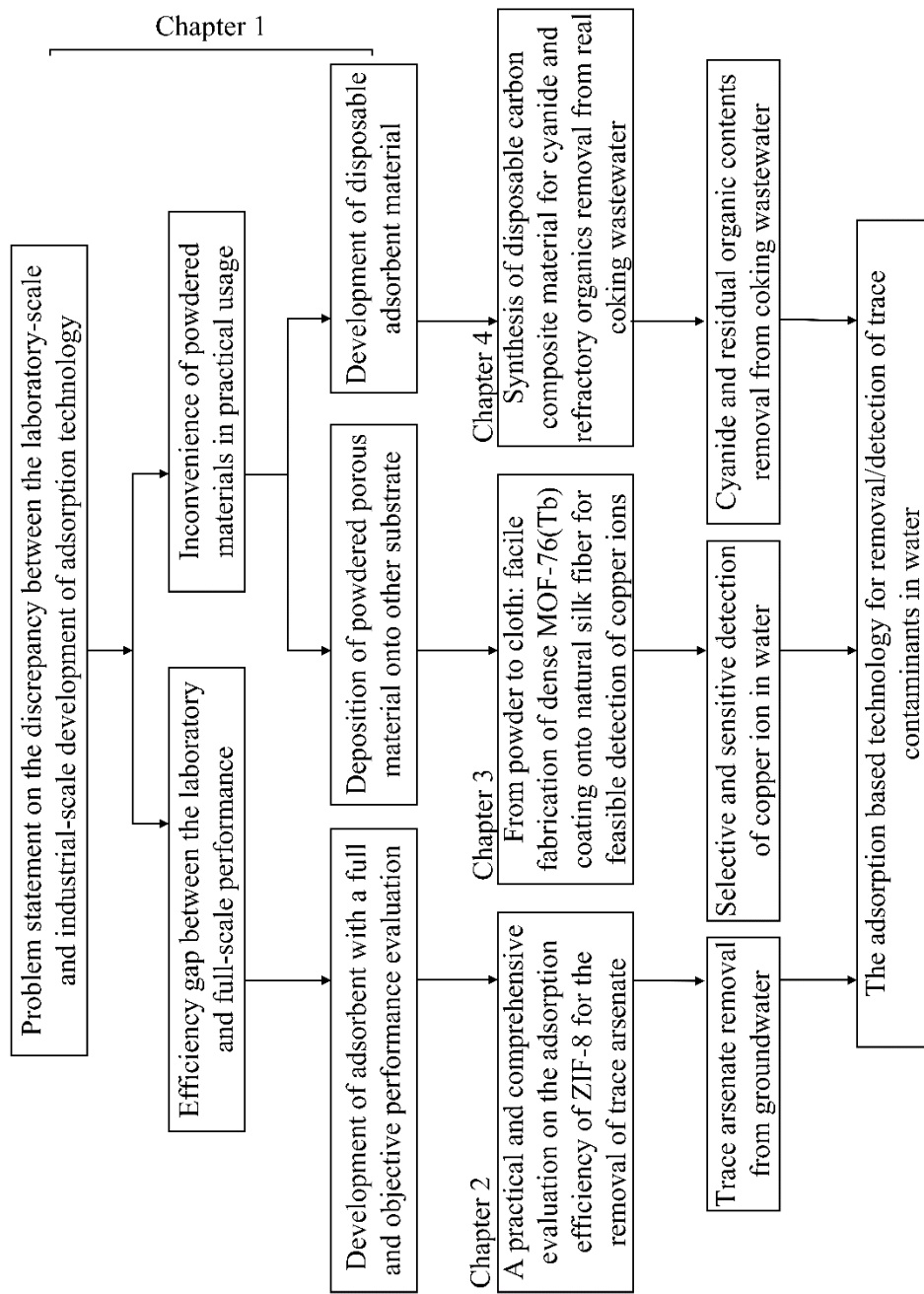
Figure 1-1. Experimental framework of this study.

Chapter 2 A practical and comprehensive evaluation on the adsorption efficiency of ZIF-8 for the removal of trace arsenate

2.1 Introduction

Traditional technologies such as coagulation, membrane technology, and adsorption are often used to treat As(V)-contaminated water. Thereinto, adsorption is an efficient method for purifying polluted water that contains recalcitrant organic pollutants and heavy metals. For the removal of trace contaminants (ppb, 10^{-9}), the adsorption method is superior to the coagulation method which requires high doses of coagulants [51]. Adsorption method also has the merits of low cost and being easy to operate, while membrane technology requires high energy consumption, tedious operation, and complex instruments [52]. In terms of adsorption technology, the main focus is to seek and explore highly efficient adsorbents.

Zeolitic imidazolate frameworks-8 (i.e., ZIF-8), in which zinc ions act as coordination centers and link together with 2-methylimidazole through self-assembly processes, constitutes an emerging class of porous materials [53]. Featured by high chemical and thermal stability, large accessible surface area and abundant active surface sites [54-56], ZIF-8 has attracted considerable attention in many applications. Typically, ZIF-8 is taken as hydrophobic material and widely used in gas storage (CO_2, CH_4, etc.) and separation of organic chemicals (benzotriazoles, organic vapors, etc.) [57-60]. The main adsorption and removal mechanism includes electrostatic enhancement, hydrophobic and π-π interaction, etc.

Indeed, due to its hydrophobic nature, the amounts of water adsorbed onto ZIF-8 are extremely low [61]. So, it seems to be unsuitable to use ZIF-8 for the adsorption and removal of aquatic arsenate. However, various degrees of hydrophilicity could be theoretically obtained with adequate functionalization of the linkers [62]. With the help of adsorption sites monitoring by DFT (density functional theory) calculations and GCMC (grand canonical Monte Carlo method) simulation, previous researches have demonstrated that acid-basic sites including the hydrogen group and amino group could be obtained at the external surface or at defects, through the dissociative adsorption of water [63, 64]. In addition, the impact of external surface area of ZIF-8 crystals, especially for water adsorption, is proven to be significant and non-negligible

since the nano-sized crystals have a good dispersibility in aquatic environment [65]. Thus, despite the overall hydrophobic nature and the smaller aperture size (11 Å × 3.4 Å) of ZIF-8 which limits the diffusion of the arsenate molecule to the inner pore structure [66], abundant active adsorption sites could be obtained at its external surface, which is helpful for the adsorption of polar arsenate molecules. This hypothesis is also supported by the results of a previous research, through which a certain adsorption capacity of ZIF-8 for micro arsenate (ppm, mg/L) was discovered [56].

In this study, as mentioned previously, the removal of trace arsenate (ppb, 10^{-9}, μg/L) was emphasized, which is one of the principal challenges in the water treatment field, and the data obtained are more approaching to reality. Effects of reaction parameters, including equilibrium concentration, pH, reaction time, coexisting anions, and adsorbent regeneration on the adsorption capacity were studied by means of single factor experiment method. In addition, through FTIR and XPS spectra, the possible mechanisms involved in the adsorption process were discussed and the key factors to the formation of the high removal efficiency were investigated.

2.2 Materials and methods

2.2.1 Materials and synthesis

2-methylimidazole, and $Zn(NO_3)_2 \cdot 6H_2O$ were purchased from Alfa Aresar; Methanol, $Na_3AsO_4 \cdot 12H_2O$, and other chemicals were supplied by Sinoreagent. All solvents and chemicals were of reagent quality and were used without further purification. De-ionized water was used throughout this work.

Based on the previously published works [67, 68], ZIF-8 was synthesized and activated with a rapid room-temperature synthetic route. Typically, 2-methylimidazole (2.2 g, 26.83 mmol) was added into methanol (100 mL) and stirred until the solid was fully dissolved. Then, $Zn(NO_3)_2 \cdot 6H_2O$ (0.5 g, 1.68 mmol) was added into the mixture and stirred at 25 °C for 8 h. The white precipitates were separated by centrifugation and washed with methanol for 3 times to remove the organic residues. Finally, the sample was dried at 150 °C overnight for further use.

2.2.2 Adsorption experiment procedures

Reaction volume was 500 mL and the adsorbent dosage was 40 mg/L for ZIF-8. Arsenate solution with different initial concentration was prepared by dissolving $Na_3AsO_4 \cdot 12H_2O$ into de-ionized water. The pH was adjusted by 1.0 M HNO_3 or NaOH solution. All experiments were conducted at room temperature (25 °C) and the flask was shaken at 150 rpm in a thermostatic shaker (WELL, HZQ-B, China). After the adsorption process, the suspension was separated by a 0.22 μm membrane. The As(V) concentration of the filtrate was determined by inductively coupled plasma (ICP) spectrometer (Agilent 720ES, USA) at ppm level (mg/L) or ICP-MS spectrometer (Agilent 7700, USA) at ppb level (μg/L). The adsorption capacity (q, mg/g) was calculated by equation (2-1).

$$q = (C_0 - C_t)V/m \tag{2-1}$$

where C_0 and C_t are the initial and residual concentrations (mg/L) of As(V), respectively; V is the volume of solution (L) and m is the mass of the adsorbent (g).

(1) Adsorption isotherms

Langmuir and Freundlich models were used to fit the adsorption isotherms. The equations are presented as follows:

Langmuir model: $\quad q_e = \dfrac{q_m C_e}{1/b + C_e}$ $\hfill (2-2)$

Freundlich model: $\quad q_e = K_f C_e^{1/n}$ $\hfill (2-3)$

where q_e (mg/g) is the adsorbed amount of As(V) at equilibrium, q_m (mg/g) is the maximum adsorption capacity, b is the adsorption constant, C_e is the equilibrium As(V) concentration (mg/L); K_f and n are an indicator of the adsorption capacity and intensity, respectively.

(2) Adsorption dynamics

To elucidate the dynamics, classic orders (pseudo-first- and pseudo-second-order models) were employed to describe the kinetic data. The equations of the two models are given as follows:

Pseudo-first-order model: $\dfrac{dq_t}{dt} = k_1(q_e - q_t)$ $\hfill (2-4)$

Pseudo-second-order model: $\frac{dq_t}{dt} = k_2(q_e - q_t)^2$ (2-5)

in which q_e (mg/g) and q_t (mg/g) are the amounts of adsorbed As(V) per mass of adsorbent at equilibrium and at time t (h), respectively; k_1 and k_2 are the related constants.

2.2.3 Batch experiment procedures

(1) Adsorption kinetics

The adsorption kinetics was studied with varying reaction time (from 5 min to 48 h). Initial As(V) concentration was 5.0 ± 0.2 mg/L, and pH was 7.0 ± 0.2.

(2) pH effect

The effect of pH on adsorption was investigated with varying initial pH (4, 6, 7, 8, and 10). Initial As(V) concentrations were 5.0 ± 0.2 mg/L and the reaction time was determined by previous kinetic data.

(3) Adsorption isotherms

Adsorption isotherms of ZIF-8 were performed with different initial As(V) concentrations (1.0, 2.5, 5.0, 7.5, and 10.0 mg/L) at an optimum pH. To get the adsorption isotherms in the condition of trace As(V) removal, samples with low initial concentrations (0.05, 0.1, 0.25, 0.5, and 0.75 mg/L) were also tested. The adsorption isotherm experiments were repeated three times.

(4) Competitive adsorption

The reaction volume was 500 mL and the dosage of the adsorbent was 40 mg/L. Initial As(V) concentration was 5.0 ± 0.2 mg/L, with the reaction time of 24 h and pH of 7.0 ± 0.2. Competitive adsorption was tested in the presence of 0.2 m mol/L single competing anion (Cl^-, F^-, NO_3^-, SO_4^{2-}, or PO_4^{3-}) to simulate the competition effect by these co-existing anions. The water samples were prepared by dissolving sodium salts (NaCl, NaF, NaNO$_3$, Na$_2$SO$_4$, or Na$_3$PO$_4$) in de-ionized water.

(5) Adsorbent regeneration

The reaction volume was 500 mL (150 rpm) and the dosage of the adsorbent was 40 mg/L. Initial As(V) concentration was 5 ± 0.2 mg/L, with the reaction time of 24 h and pH of 7.0 ± 0.2. After adsorption, the adsorbents with known amount of arsenate were collected by filtration

and washed with de-ionized water. Then, the adsorbents were placed into different solution (NaOH, NaCl, HNO$_3$, and Methanol) and shaken for 12 h for desorption. By comparing the amounts of the desorbed arsenate and the stability of ZIF-8 in the corresponding regeneration agent, the most suitable solution for regeneration was selected. At last, the adsorbent was filtered and dried for recycle use. The regeneration cycles were repeated for three times. The adsorption capacity and desorption amount of arsenate were calculated (concentration difference multiplied by the volume) in each regeneration recycle.

(6) Sample preparation for FTIR and XPS

20 mg ZIF-8 was added into 500 mL arsenate solution (5 mg/L). Reaction time was 24 h and the solution pH was 7.0±0.2. The As-loaded adsorbents were collected by filtration and washed with de-ionized water. After dehydration, the As-loaded ZIF-8 was prepared for further FTIR and XPS analysis. The preparation of ZIF-8 before adsorption was subject to the above treatment process in the absence of arsenate.

2.2.4 Material characterization

The crystal structure of the adsorbents was obtained by an X-ray powder diffractometer (D8 Advance, Germany). The BET surface area of the adsorbent was obtained with ASAP2020M analyzer (Micromeritics, USA) at 77 K in the relative pressure range of 0.05~0.25. The scanning electron microscope (SEM) and transmission electron microscope (TEM) images were obtained by Hitachi S4800, Japan and Tecnai G2 F20 S-TWIN, USA, respectively.

The zeta potential of the adsorbent at different pH was measured by a Zeta potential analyzer (Zetasizer Nano ZS 90, United Kingdom). The Fourier transform infrared (FTIR) spectra of the adsorbent before and after adsorption were obtained on a FTIR spectrophotometer (Nicolet 5700, USA). The adsorbent samples before and after arsenic adsorption were analyzed using an X-ray photoelectron spectroscope (AXIS Ultra DLD, Kratos, Japan) with a 1486.6 eV Al Kα X-ray source. The energy step size for the wide-scan spectra and high-resolution scan were 1 and 0.05 eV, respectively. To compensate the charging effects, all binding energies were calibrated with neutral C$_{1s}$ at a binding energy of 284.6 eV. The spectra peaks were fitted using XPSPEAK41 software.

2.3 Results and discussion

2.3.1 Characterization of the synthesized ZIF-8

In comparison of the XRD patterns of the synthesized material to the simulated pattern of ZIF-8 (Fig. 2-1), all the characteristic peaks highly agreed with a SOD type of ZIF-8 structure. The BET surface area of the synthesized ZIF-8 was 1388 m^2/g (Fig. 2-2). Fig. 2-3 and 2-4 show the representative SEM and TEM images of the synthesized ZIF-8, respectively. To conclude, our straightforward synthetic route yields pure-phase ZIF-8 nanocrystals with a narrow size distribution and large accessible surface area.
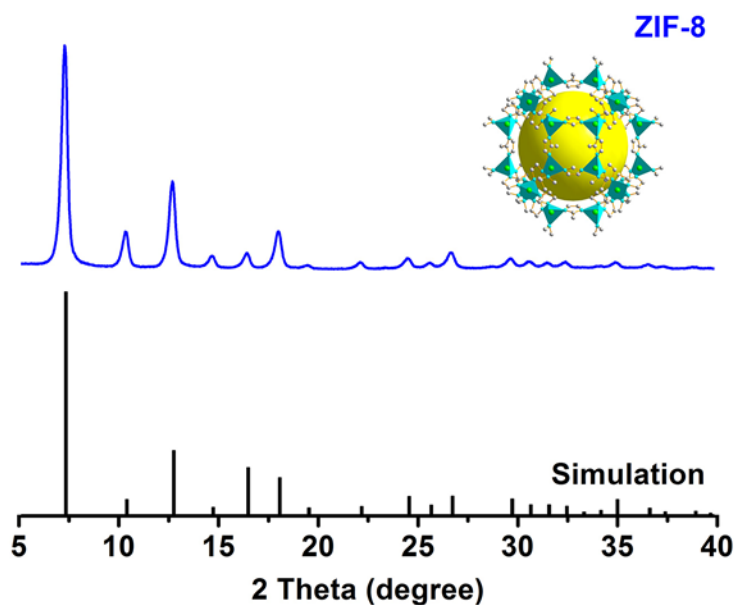
Figure 2-1. XRD patterns of the simulated and the prepared ZIF-8.
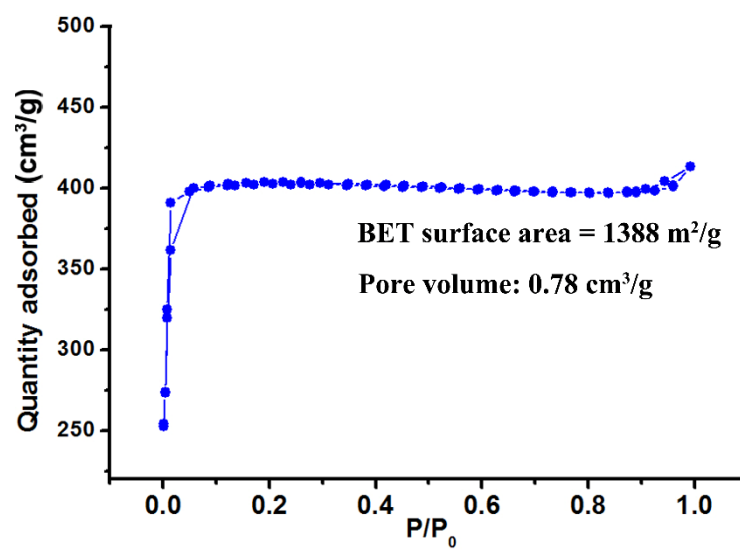
Figure 2-2. N$_2$ adsorption-desorption isotherm of the prepared ZIF-8.
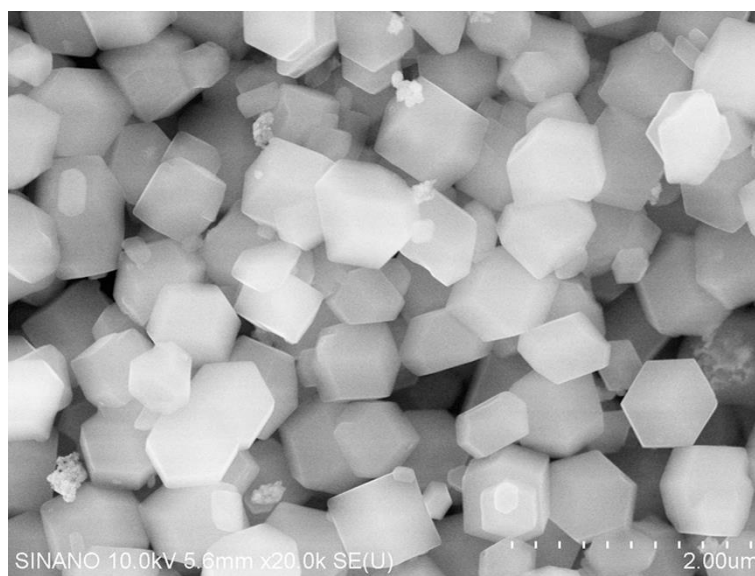
Figure 2-3. SEM image of the prepared ZIF-8.
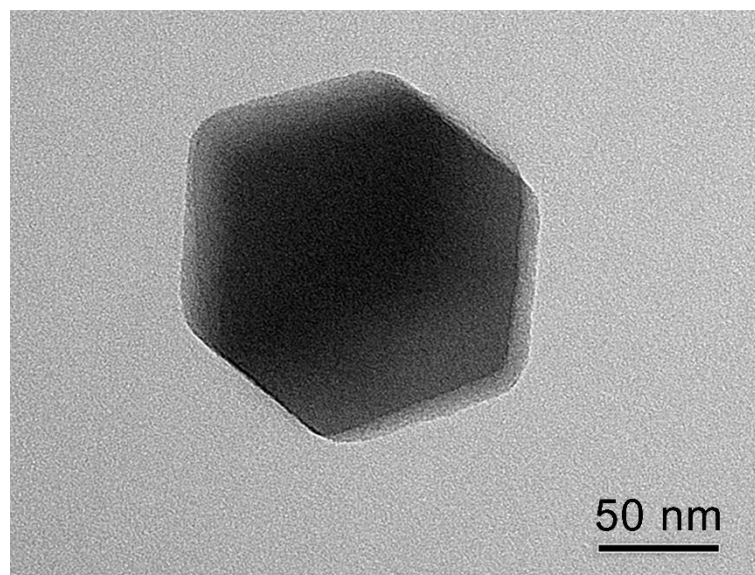
Figure 2-4. TEM image of the prepared ZIF-8.

2.3.2 Adsorption isotherms

The adsorption isotherms data with fitting models are shown in Fig. 2-5. High correlation coefficients (R^2, in Table 2-1) suggest that Langmuir model is suitable for describing As(V) adsorption onto ZIF-8. The maximum removal capacity of ZIF-8 from the corresponding model is 106.7 mg/g, in good agreement with the actual experimental results. The equilibrium adsorption isotherm can directly yield the conditional removal capacity to enable comparison between various adsorbents [69]. However, the removal capacity is affected by many factors, such as reaction time, competitive ions, pH and, equilibrium concentration; the latter considerably affects the adsorption capacity because an increased adsorbate concentration implies a high driving force and an enhanced interaction process [70]. Too often, there's no comparison between the arsenic concentrations in natural water and those employed in various previously reported works [71]. As a result, there is a wide gap between the model-obtained result and the actual removal capacity in real practice. To conclude, directly comparing the adsorption capacity and ignoring the differences in equilibrium concentrations can't achieve objective evaluations.
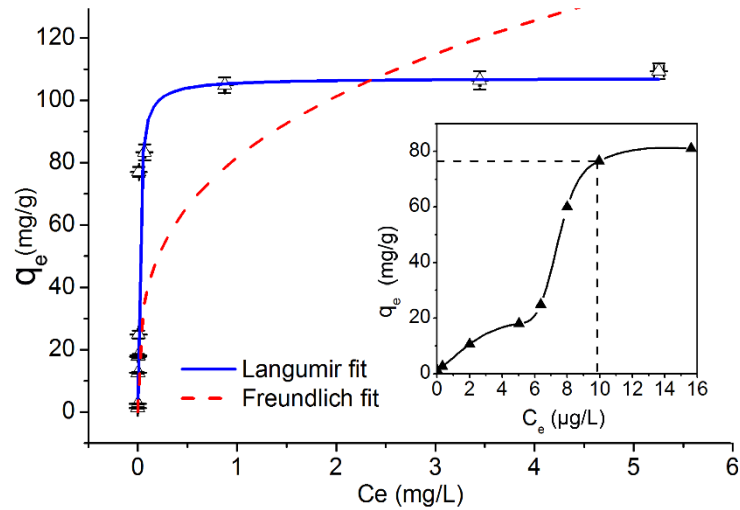
Figure 2-5. Adsorption isotherms of As(V) onto ZIF-8. The inset shows the high-resolution isotherm at extremely low equilibrium concentrations.

Table 2-1. Parameters obtained from the adsorption isotherms of As(V) onto ZIF-8.

	Langmuir model			Freundlich model		
adsorbent	q_{max}(mg/g)	b	R^2	K_f	n	R^2
ZIF-8	106.70	85.40	0.940	90.31	5.65	0.790

To further study the removal capacity of trace arsenate, the adsorption isotherm of As(V) onto ZIF-8 under extremely low equilibrium concentrations is shown as an inset in Fig. 2-5. At an equilibrium concentration of 9.8 µg/L (below the safety limit for arsenic in drinking water revised by the World Health Organization and U.S Environmental Protection Agency, meaning that the treated water does not need any further purification after the adsorption), ZIF-8 exhibited a capacitiy of 76.5 mg/g which is the first and highest reported adsorption capacity (Table 2-2), indicating that ZIF-8 is a promising alternative adsorbent for trace As(V) removal from water.

Table 2-2. Comparison of adsorption capacities of As(V) on various adsorbents.

Adsorbent	Equilibrium concentration (μg/L)	Capacity (mg/g)	Publication year
Fe_3O_4 nanocrystals	7.8	0.98	2006 [72]
Nano Fe-Cu binary oxide	9.7	37.0	2013 [73]
Powder Ce–Ti sorbent	10	7.5	2010 [71]
Granular Ce–Ti sorbent	10	2.5	2010 [71]
Granular ferric hydroxide (GFH)	10	8.0	2004 [74]
ZIF-8	9.8	76.5	This study

In addition, in the first half of the "S"-shaped nonlinear isotherms, the increased ratio of the adsorbed As(V) amount (mg/g) to the equilibrium As(V) concentration (μg/L) suggests increased adsorbate affinity as a function of surface As(V) concentration. The above phenomena indicates that cooperative interactions between As(V) species (e.g., van der Waals force and hydrogen bonding) may occur at low surface coverage and depicts an active capture process of As(V) species instead of the random adsorption [75]. This hypothesis is contrary to the Langmuir model that a uniform monolayer adsorption and no reactions between As(V) species are assumed. In fact, however, only in wide concentration range can Langmuir model obtain a stable maximum adsorption capacity and a good simulation result. The adsorption isotherms under extremely low concentration range just make up for the inapplicability of the Langmuir model at low concentration range and give a detailed display of the adsorption performance in the whole concentration range. For the cooperative interaction between As(V) species, it is conspicuous at low surface coverage (seen through in the form of 'S'-shaped isotherm) and gradually diminished by increasing amounts of chemical adsorption with higher adsorbate concentrations, as illustrated in the form of stable capacity line of Langmuir model isotherm.

2.3.3 Proposed mechanism of As(V) adsorption onto ZIF-8

To elucidate the As(V) adsorption mechanism, the FTIR and XPS spectra were obtained before and after As(V) adsorption. Fig. 2-6 illustrates the FTIR spectra of pristine and As-loaded adsorbent. The primary peaks match well with previously reported results [54]. The spectra of ZIF-8 before and after adsorption are similar except for some new peaks. The broad peak at 3387 cm^{-1} is ascribed to the stretching vibration of hydroxyl and amino groups, which are difficult to distinguish and separate completely. Abundant surface active sites including Zn-OH and N-H are produced through the dissociative adsorption of water [55, 63], in good agreement with the hypothesis previously mentioned. The intense peak at 844 cm^{-1} is assigned to the stretching vibration of As-O, indicating the successful adsorption of As(V) species onto ZIF-8 [76]. The absorption peak near 500 cm^{-1} is characterized by metal-oxygen vibration [71].
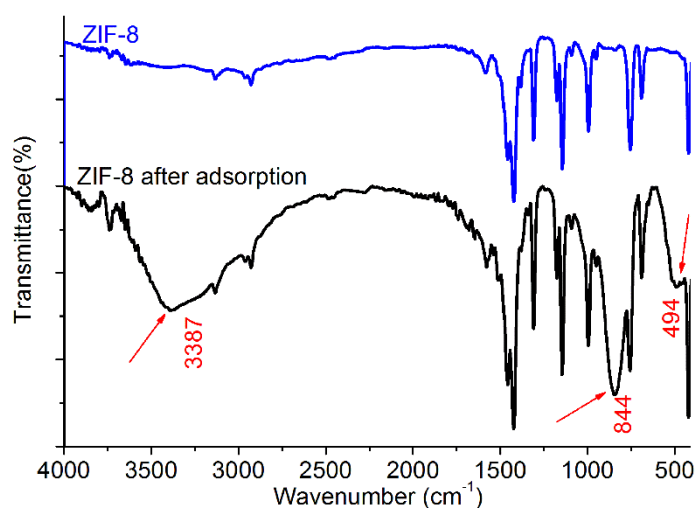
Figure 2-6. FTIR spectra of ZIF-8 before and after As(V) adsorption.
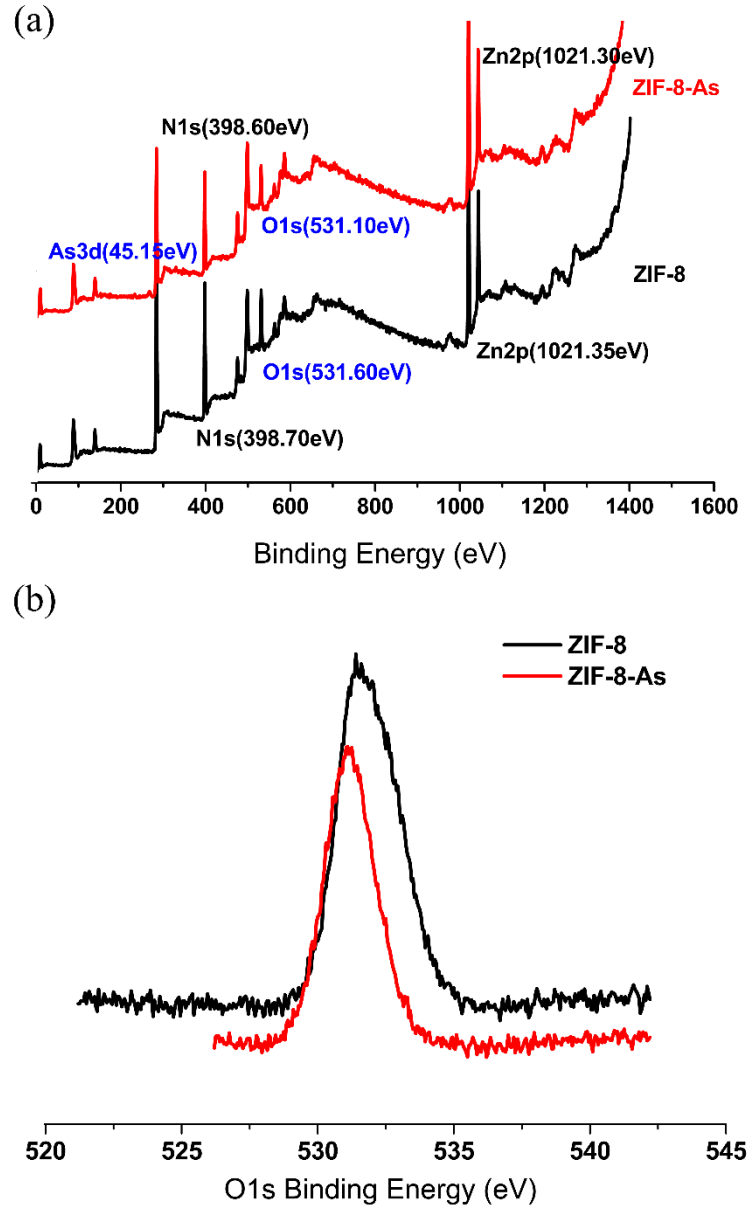
Figure 2-7. XPS spectra of ZIF-8 before and after As(V) adsorption. (a) Wide scan spectra; (b) O1s spectra with high resolution.

The wide-scan XPS spectra (Fig. 2-7a) reveals that some arsenic atoms are detected on the surface after adsorption, confirming the successful adsorption of As(V). Among the binding energy peaks, only O1s peak decreased considerably from 531.6 to 531.1 eV (Fig. 2-7b). Fig. 2-8 illustrates the deconvoluted spectra of the O1s region to analyze the adsorption mechanism. The O1s spectra of virgin ZIF-8 (Fig. 2-8a) produced H_2O and M-OH (Zn-OH) peaks at 533.55 and 531.73 eV, respectively [77]. After adsorption (Fig. 2-8b), a new peak appeared with a

binding energy of 530.90 eV and represented M-O-M [71]. Despite the fact that As-OH group contained in the arsenic species (H_3AsO_4, $H_2AsO_4^-$, and $HAsO_4^{2-}$) should have increased the fraction of surface hydroxyl group [71], the area ratio of M-OH decreased from 91.40% to 34.40% after As(V) adsorption, indicating the involvement of hydroxyl group and chemical adsorption process of As(V) onto ZIF-8.
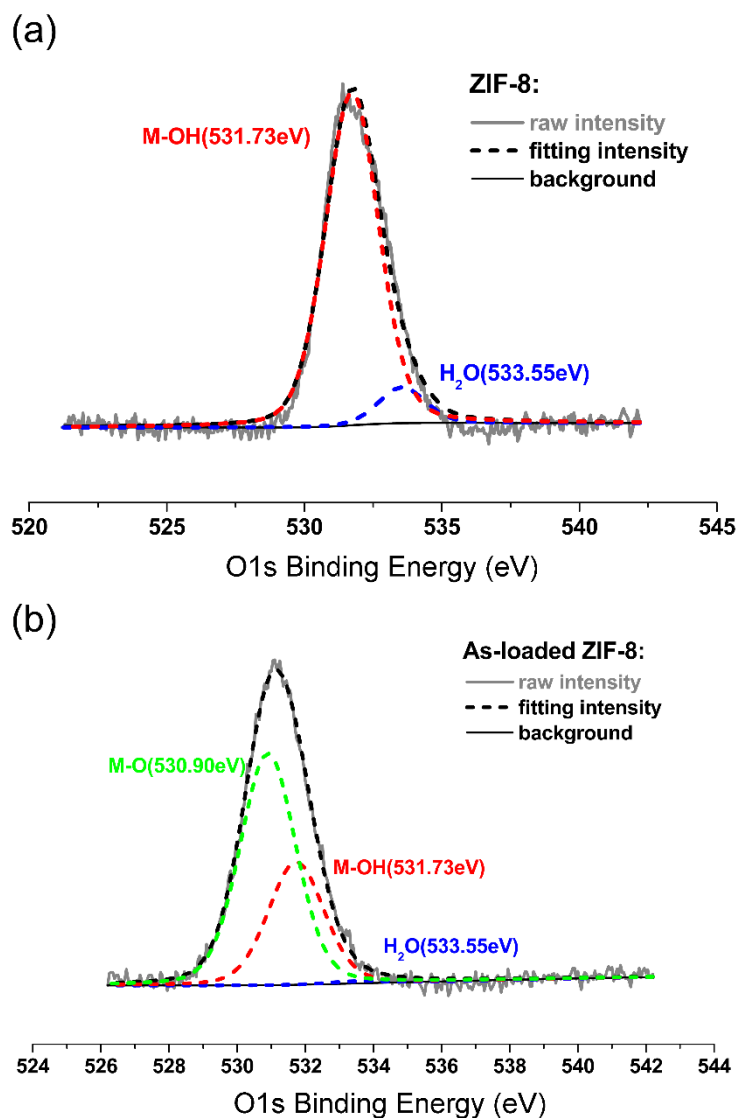
Figure 2-8. Deconvoluted O1s spectra of ZIF-8 before (a) and after (b) As(V) adsorption. Full and dashed lines represent the raw intensity data and the deconvolution fitting intensities, respectively.

In summary, the proposed mechanism of As(V) adsorption onto ZIF-8 is mainly related with the following two aspects: (1) production of large amount of external active sites (Zn-OH)

through the dissociative adsorption of water, and (2) subsequent formation of an inner-sphere complex (e.g., monodentate and bidentate complexes) (Fig. 2-9) [78]. To explain the previous study of FTIR spectra, a new peak at 500 cm^{-1} is attributed to the M-O-M bond (Zn-O-As), implying the formation of arsenic-contained inner complex.
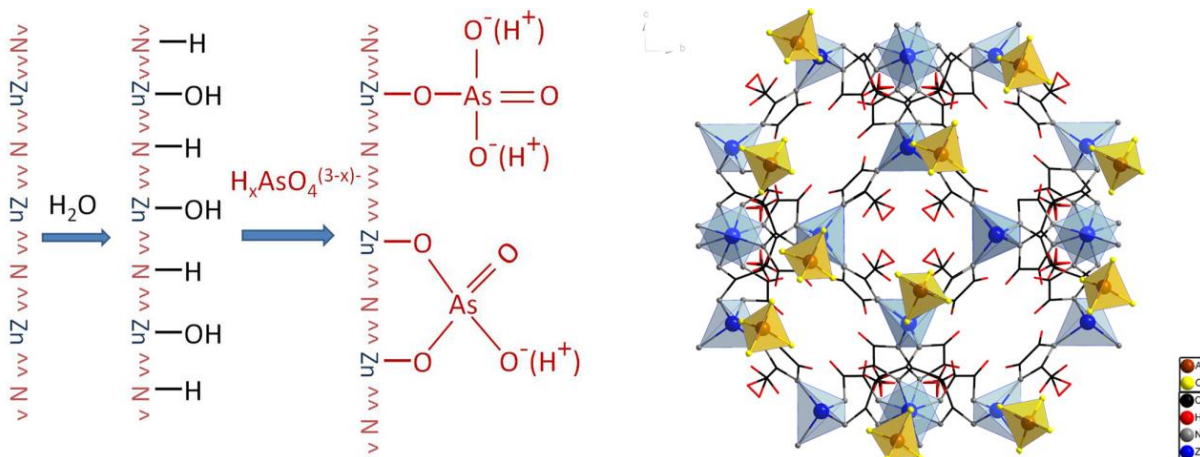
Figure 2-9. Proposed adsorption mechanism and simulated locations of As(V) molecules onto ZIF-8. Colour scheme: Zn, blue; O, yellow; N, gray; C, dark; H, red; and As, brown. All metal ions and arsenate are present as the polyhedral.

2.3.4 Conditional adsorption properties

Fig. 2-10 illustrates the effect of adsorption time on the removal of As(V). Higher correlation coefficients (R^2, in Table 2-3) indicate that the experimental data fit better to the pseudo-second-order model, which assumes chemical adsorption process and that the adsorption rate is controlled by two factors: adsorbate concentration and the surface properties of the adsorbent. The adsorption rate was initially high and slowed down thereafter. ZIF-8 reached 50% of its adsorption capacity within 3 h and up to 80% of the maximum removal capacity was finished within 12 h. In general, the adsorption rate is lower compared to the reported adsorption process of organic chemicals [60]. The following reasons might be responsible for this relatively slow rate: the chemical arsenate adsorption process is usually slower than physical adsorption processes; in addition, before the chemical adsorption process, the hydration process to form surface hydrogen group by dissociative adsorption of water also needs some time [79].
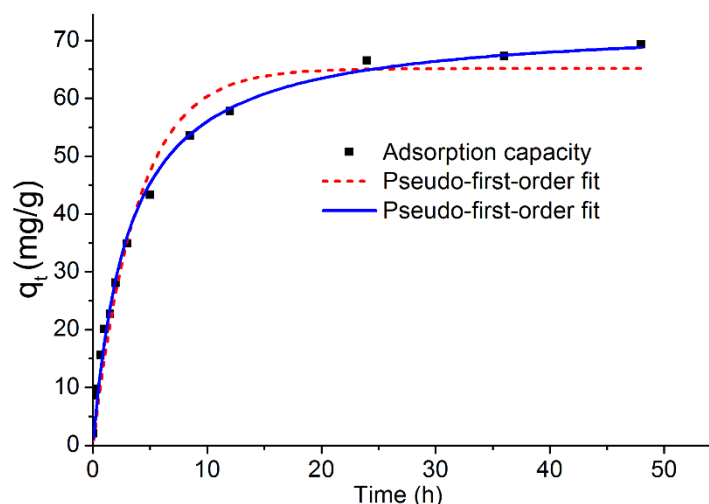
Figure 2-10. Adsorption kinetic of arsenate onto ZIF-8.

Table 2-3. Adsorption kinetic constants obtained from different models.

	Pseudo-first-order model			Pseudo-second-order model		
adsorbent	k_1(1/min)	q_e(mg/g)	R^2	k_2(g/mg/min)	q_e(mg/g)	R^2
ZIF-8	0.26	65.14	0.971	0.004	73.20	0.992

As(V) uptake is analyzed as a function of the initial pH (Fig. 2-11) to determine the optimum pH for As(V) adsorption. The removal capacity steadily increased with the decrease in pH and reached the maximum capacity at pH 4.0. Solution pH affects the performance of the adsorbents because it would not only influence the surface charge indicated by zeta potential of the material in this study but would also control the As(V) speciation during adsorption. Aquatic As(V) mainly exists as H_3AsO_4, $H_2AsO_4^-$, $HAsO_4^{2-}$, and AsO_4^{3-} when pH < 2.3, =3~6, 8~10.5, or > 11, respectively, for various ionization degrees [80, 81]. The point of zero charge (pH$_{zpc}$) for ZIF-8 is at pH 9.3. Reducing the pH could reverse the surface charge from negative to positive, which is conducive to the adsorption of negatively charged pollutants. However, the negative charge of As(V) species reduces from divalent to monovalent upon reduction in pH and even reaches zero valence from the reduction. The above beneficial and converse effects are supposed to be compromised, yielding an optimum pH value. Interestingly, for ZIF-8, the removal capacity steadily increased with the decrease of pH; the capacity depended neither on

the surface charge of the adsorbent nor on the negative charge of As(V) species. Thus, some other forces should have diminished the impact of electrostatic attraction. Considering the chemical adsorption process that through ion exchange to form inner-complex, the increased adsorption capacity at low pH mainly benefits from increased amount of hydroxyl group in As(V) species under acidic conditions.
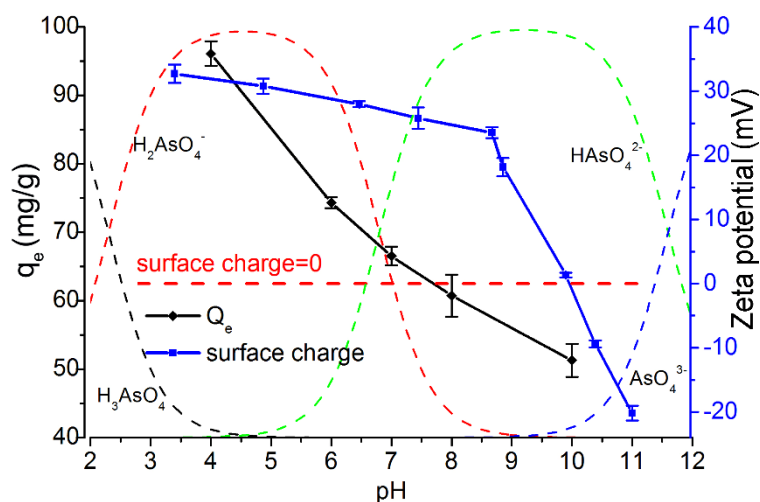
Figure 2-11. pH effects on adsorption capacity and zeta potential of ZIF-8.

In natural water, various ions often coexist with arsenate. In this section, several common anions (Cl^-, F^-, NO_3^-, SO_4^{2-}, and PO_4^{3-}) were selected to analyze their effects on the removal efficiency (Fig. 2-12). Only 18.8% of the maximum removal capacity was remaining in the presence of PO_4^{3-} (0.2 m mol/L), indicating the marked inhibitory effect of PO_4^{3-} due to its similar nature to AsO_4^{3-}, and their competition for binding sites. However, it should be noted that the adverse effects would not be so serious since the mass ratio of PO_4^{3-} to AsO_4^{3-} amount is much lower in natural water. The existence of F^- also exhibited some negative impact on As(V) removal. Other ions failed to show remarkable influence on the adsorption performance of ZIF-8. The inhibitory effects of the ions on the adsorption capacity followed a descending order as: $PO_4^{3-} > F^- > SO_4^{2-} > NO_3^- > Cl^-$. To conclude, the coexisting anions do have some negative effect on the adsorption efficiency and the results are generally in agreement with a previous study [81]. The difference is that, compared to other materials, the impact on adsorption efficiency is greater with the existence of the coexisting anions, especially for PO_4^{3-}.
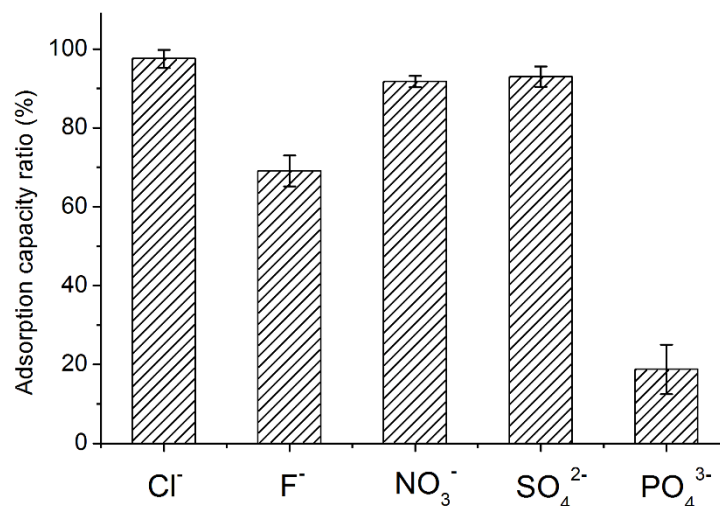
Figure 2-12. Effects of competition anions on adsorption capacity.

To study the regeneration ability of ZIF-8, HNO_3, HCl, NaCl, NaOH, and methanol solutions were used to regenerate As(V)-loaded material; 0.02 M NaOH was chosen finally. Fig. 2-13 reveals that ZIF-8 maintained greater than 80% of its capacity after three recycling times. The desorption of As(V) from ZIF-8 is ascribed to the ion exchange between As(V) species and abundant hydroxyl groups. The loss of adsorption capacity results from some inactive sites occupied by some undesorbed arsenate molecular since the desorption cannot be achieved completely; Also, despite the overall stability of the crystalline structure, some minor collapse of the crystalline structure, confirmed by the zinc ions leakage detected in the filtrate, leds to the decrease of zinc centers which can produce active surface hydrogen group. In general, after three regeneration cycles, the adsorption capacity of ZIF-8 can be maintained at a comparatively high level with only a slight decrease of its adsorption capacity (17%).
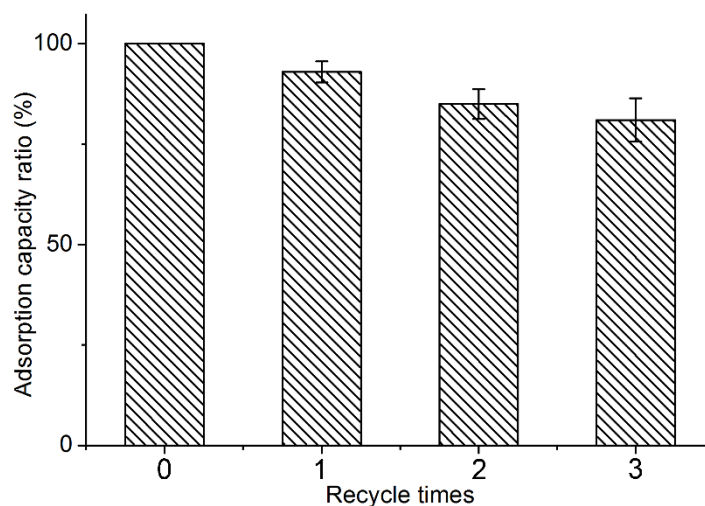
Figure 2-13. Adsorption capacity ratios in three recycle times.

2.3.5 Characterization of ZIF-8 after the adsorption

As shown in Fig. 2-14, the intensity of the characteristic peaks weakened dramatically, indicating large decrease in crystallinity. The above conclusion is supported by the SEM image of ZIF-8 after adsorption (Fig. 2-15), which shows obvious cluster effect and decreased crystallinity. As a result (Table 2-4), the mesopore volume increased from 0.11 m^3/g to 0.83 m^3/g for the formation of accumulated mesopore. In contrast, the surface area and micropore volume decreased slightly (from 1388 m^2/g to 1246 m^2/g, 0.66 m^3/g to 0.55 m^3/g, respectively), consistent with the hypothesis that the binding sites are mostly at the external surface. So, the slight decrease of surface area and micropore volume results from the surface coverage instead of internal filling of the micropore.
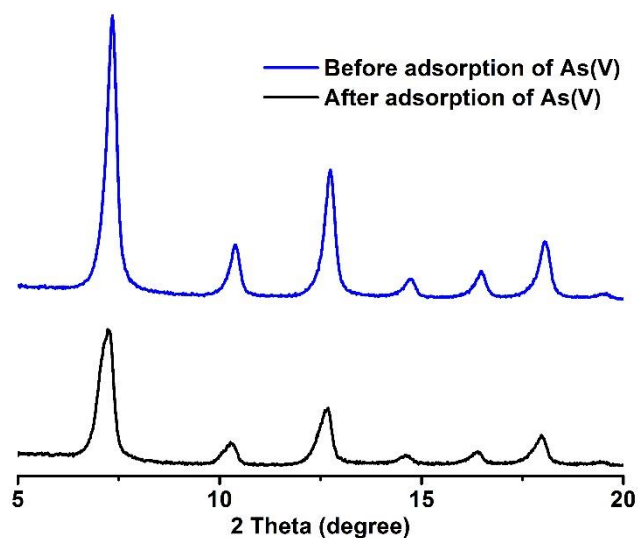
Figure 2-14. XRD patterns of the pristine ZIF-8 and that after the adsorption of As(V).
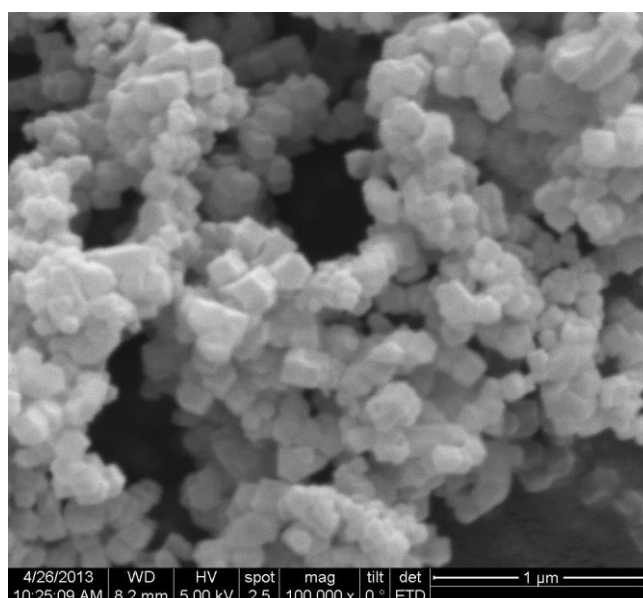
Figure 2-15. SEM image of ZIF-8 after the adsorption of As(V).

Table 2-4. Characterization of the ZIF-8 before and after adsorption

	Before adsorption	After adsorption
BET surface area	1388 m^2/g	1246 m^2/g
Micropore volume	0.66 m^3/g	0.55 m^3/g
Mesopore volume	0.11 m^3/g	0.83 m^3/g

2.4 Summary

In this work, a more practical and comprehensive evaluation system was put forward, which gave full consideration of material's adaptability to water environment (pollutant concentration, pH, coexisting ions), adsorption rate, and regeneration capacity. To this end, the characteristics of arsenate removal from water by ZIF-8 were studied and the possible mechanisms involved in the adsorption process were discussed. The high efficiency is attributed to three key factors: (1) the hydration process to form surface hydrogen group by dissociative adsorption of water, which helps to bind As(V) species tightly onto the surface; (2) the high accessible surface area, fundamental to supply abundant adsorption sites; and (3) the cooperative interaction (e.g., Van der Waals' force and hydrogen bonding) between As(V) species at low surface coverage. ZIF-8 as an efficient adsorbent for the removal of trace As(V) presents a new material with high application potential for trace As(V) removal in practical water treatment. More extensive investigation on using ZIF-8 as a novel adsorbent is suggested for its application in the practice of water purification.

Chapter 3 From powder to cloth: facile fabrication of dense MOF-76(Tb) coating onto natural silk fiber for feasible detection of copper ions

3.1 Introduction

Metal–organic frameworks (MOFs), in which metal ions act as coordination centers and link together with organic ligands through self-assembly processes [82], have been extensively studied for various applications in the past two decades [83, 84]. Recently, lanthanide-based MOFs, one type of MOFs materials possessing unique luminescence properties such as high luminescence quantum yield, long-lived emission, large Stokes shifts, and characteristically sharp line emissions [85-87], have attracted considerable attention due to their marketable potential for chemical sensing [88-90]. In theory, the combination of luminescence and accessible porosity within MOFs confers these materials with detection capacity through the luminescence intensity change [89], thus making them become promising candidates in chemical sensing. Among the various kinds of lanthanide-based MOFs materials that have been developed, $Tb(BTC)(H_2O)_{1.5}(DMF)$ labeled as MOF-76(Tb), outperforms other materials due to its simple work-up procedure, mild reaction conditions, high yield, and high purity [91]. Furthermore, owing to its luminescent properties, MOF-76(Tb) has been explored for detection of F^- [92], U(VI) [93], aromatic pollutants [94], and small organic molecules [95, 96], etc., thus, exhibiting promising detection potential.

Although the usage of luminescent MOFs for sensing has been attempted, the inherent characteristics of powdered materials are considered to restrict their further application in real practice. Especially, fluorescent sensing in the homogeneous phase is not suitable for enrichment and removal of target species [97-99]. To date, MOFs as components of a commercial functional sensing device, have not been reported [100]. When being used as sensors, catalytic coatings, filters, or other devices, the deposition of MOFs onto solid substrate is essential and recognized as one of the most critical issues [101-104]. Some trials have been done to prepare a luminescent MOFs material-coated magnetic sphere, for easy recycling of the sensor material [88]. Meanwhile, considerable work has been done on deposition of thin MOFs films onto different substrates, such as polyester fabric [105], pulp fibers [106], and porous

alumina [101], yielding suitable materials for sensors. For all these substrate materials, however, their functionalization through atomic layer deposition (ALD) coating or formation of self-assembled monolayers (SAMs) is required as pretreatment [107], thereby increasing the complexity and cost of the whole process.

The silkworm fibroin (domestic silk), mainly consisting of glycine, alanine and sericine [108], is a fibrous protein and has been universally established as one kind of textile fibers due to its unique handle and mechanical properties. The repeated -Gly-Ala-Gly-Ala-Gly-Ser- motif in fibroin contributes a lot to the strength and stiffness of the silk, through the formation of high volume fraction of β-sheet microcrystallites [109]. In addition, theoretically, no functionalization or pretreatment is needed when fibroin fiber is used as the substrate because the reactive carboxylic groups are abundant on its surface, which are essential for the deposition of the initial MOFs layer [90, 110, 111]. Whereas further verifications for its solvent resistance and thermal stability are necessary because these properties generally dictate the possible utilization of composite in practice. Given that the procedure for deposition usually determines the quality of the coated MOFs layer, various synthesis methods can be applied for the deposition of MOF material onto the silk fibroin fiber [105, 112], which may offer different coating efficiency and performance.

Copper (II) (Cu^{2+}) is a typical micronutrient element. Excessive exposure to copper should be avoided due to its negative impact on human health [113]. However, copper pollution in waterbodies has frequently occurred in the past decades because of uncontrolled anthropogenic activities [114]. Thus, highly sensitive and selective methods for fast and reliable sensing of Cu^{2+} are crucial for water environment protection and human health safety. Among the various methods developed for the detection of trace copper in aquatic environment, the fluorescence-based method shows considerable application potential because of its simplicity, quick response time for on-site analysis, and cost-effective instrumentation, which can be easily assembled in small and low-power packages [88, 97, 115, 116].

In this work, natural fibroin fiber was selected as the substrate for the deposition of MOF-76(Tb). The solvent resistance and the surface property of the silk substrate were investigated. The coating efficiency of three methods, namely hydrothermal (HT), microwave assisted

(MWA), and layer-by-layer (LBL) methods were compared with related factors being analyzed. In addition, this work for the first time, demonstrated the extended usage of the MOF-76(Tb)@silk fiber composite for fluorescent/colorimetric sensing of copper ion (Cu^{2+}).

3.2 Materials and methods

3.2.1. Materials

All materials and chemicals were of reagent grade and used without further purification. Terbium nitrate hexahydrate and 1,3,5-benzenetricarboxylic acid were purchased from Alfa Aesar. Metal nitrates (potassium nitrate, sodium nitrate, aluminum nitrate, iron nitrate, calcium nitrate, lead nitrate, nickel nitrate, zinc nitrate, cadmium nitrate, and copper nitrate) and organic solvents (ethanol, methanol, N,N-dimethylformamide (DMF), and n-hexane) were supplied by Sinoreagent. Silkworm cocoons were purchased from a local silk farm in China. Deionized water was used throughout this work.

Silk fibroin fiber was prepared from silkworm cocoon through a degumming procedure, so as to remove the coat of sericin proteins [117-119]. The degumming treatment was processed according to a previous study [109]. The procedure was as follows: the silkworm cocoons were first rinsed in water to get rid of the surface contaminants and were then cut into small fragments with an average size of 1 cm^2. Then, the silk fiber was degummed in boiling water for 30 min. In order to ensure the maximum sericin removal, the fine fibers were further degummed in a 0.1M Na_2HCO_3 solution at 90~100 $^\circ$C for 30 min and washed with deionized water for 3 times. Finally, the sample was dried at 100 $^\circ$C for 6 h before testing and further usage.

3.2.2. Material characterization

Fourier transform infrared (FTIR) spectra of the silk fiber, before and after immersion were obtained using a FTIR spectrophotometer (Nicolet 5700, USA). Scanning electron microscopy (SEM) images were observed using a field emission scanning electron microscope (FESEM) on a JEOL JSM-5400 system, at an accelerating voltage of 15 kV. The mechanical property of the silk fiber was measured by an electronic universal testing machine (UTM 2502, China). The crystal structure of the coated material was obtained by X-ray powder

diffractometer (XRD, D8 Advance, Germany), and the data were processed in a continuous scanning mode within the range of 3~50 $^{\circ}$, at a step width of 0.02 $^{\circ}$ and scanning speed of 5 $^{\circ}$/min.

3.2.3. Preparation of MOF-coated silk fibers

Three synthesis methods, i.e. HT, MWA and LBL, were applied for MOF-coated silk fiber preparation and then compared in this study.

In the typical HT method, 0.120 g of $Tb(NO_3)_3 \cdot 6H_2O$ (0.28 mmol) and 0.020 g of H_3BTC (0.10 mmol) were dissolved in the mixture of DMF (4.0 mL), ethanol (4.0 mL), and H_2O (3.2 mL). Then, the reaction mixture was stirred for 1 h and later poured into a solvothermal vessel containing 70 mg of silk fiber. The vessel was sealed and heated to 80 $^{\circ}$C at a rate of 2 $^{\circ}$C/min for 24 h to obtain white precipitates. The obtained materials were washed with ethanol and dried at 80 $^{\circ}$C in vacuum for further use [120].

In the typical MWA synthesis [94], the same mixture solution used in the HT method was transferred into a microwave vessel containing 70 mg of silk fiber. Then the vessel was sealed and heated to 80 $^{\circ}$C at a heating rate of 2 $^{\circ}$C/min for a certain amount of time. The obtained white precipitates were washed thrice with ethanol and then dried in vacuum for further use.

In the typical preparation by the LBL method [121], a mixture of $Tb(NO_3)_3 \cdot 6H_2O$ (0.120 g, 0.28 mmol), DMF (4.0 mL), ethanol (4.0 mL), and H_2O (3.2 mL) was termed as the precursor solution A. The precursor solution B was the mixture of H_3BTC (0.120 g, 0.28 mmol), DMF (4.0 mL), ethanol (4.0 mL), and H_2O (3.2 mL). The weighed silk fibers (70 mg) were dipped in solutions A and B for 4 h, alternatively. After each dipping, the silk fiber was rinsed in ethanol to remove the unreacted precursor. After a few preparation cycles, the samples were dried in vacuum for further use.

3.2.4. Luminescent sensing procedures

All the luminescence sensing measurements were performed at room temperature by a Horiba FluoroMax-4 spectrofluorophotometer with the range of 450~650 nm having a fixed excitation wavelength of 303 nm. The luminescence intensity was evaluated by the intensity of the strongest emission ($^5D_4 \rightarrow {}^7F_5$ transition) at 548 nm. The quenching effect was determined by the intensity variation of the MOF-76(Tb)@silk fiber composite before and after the addition

of analyte solution.

3.3 Results and discussion

3.3.1. Surface properties of silk fiber and its solvent resistance

The SEM image (Fig. 3-1a) reveals the flattened shape of the pristine silk fiber at a high magnification, the smooth surface of which, in theory, makes it a good fit for coating MOFs material with low roughness [105]. In the IR spectra (Fig. 3-1b), the broad peak at 3294.6 cm^{-1} (O–H stretching) and the intensive peak at 1678.4 cm^{-1} (C=O stretching) were ascribed to the stretching vibration of surface carboxylic groups formed from the polymerization of typical amino acids like glycine and alanine [122-124]. The abundant carboxylate linkers on the surface of silk fiber suggest its great potential for coating MOFs material, as functionalization of the substrate surface is essential for the formation of MOFs coating [105, 112].
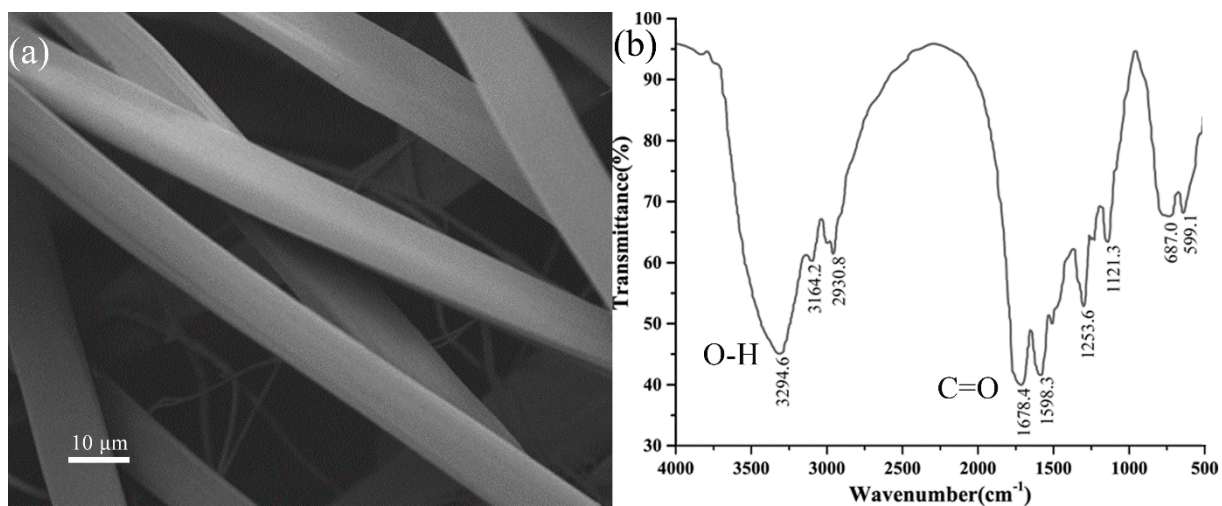
Figure 3-1. SEM image (a) and FTIR spectra (b) of the natural silk fibers used in this work.

To explore the thermal stability and solvent endurance of the silk fiber, the surface and mechanical properties were compared between the raw material and those after being immersed into the commonly used solvents (water, DMF, ethanol, and n-hexane) at 80 °C (the synthesis temperature for MOF-76(Tb)). As shown in Fig. 3-2a, the primary peaks matched well with the raw material, indicating that the main surface functional groups could be maintained after immersion into the tested solvents (polar or nonpolar, organic and inorganic solutions) for 24 h. In addition, each fiber was well proportioned, with a smooth surface and devoid of any

apparent deformation, fracture, fold, or swelling (Fig. 3-3), thereby maintaining the structural properties of the raw silk fiber. In terms of mechanical property, although the tensile strength showed some slight decrease after immersion in the above mentioned solvents (Fig. 3-2b), the residual tensile strength (1.730 MPa, 1.749MPa, and 1.521MPa in water, methanol, and DMF, respectively) was sufficient for further coating operation and application of the composite material in real practice.
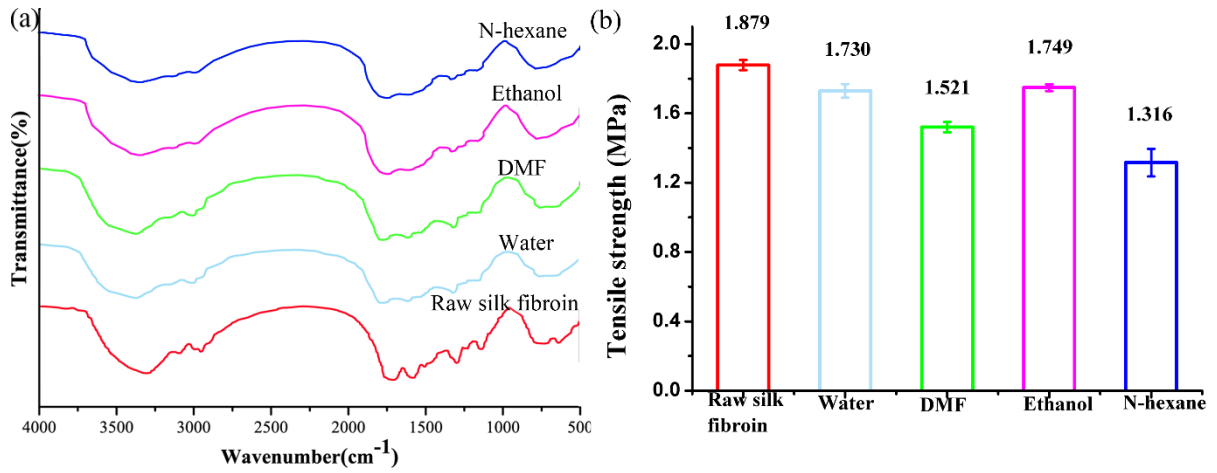
Figure 3-2. FTIR spectra (a) and comparison of the tensile strength (b) of silk fiber before and after immersion in various solvents at 80 °C for 24 h.
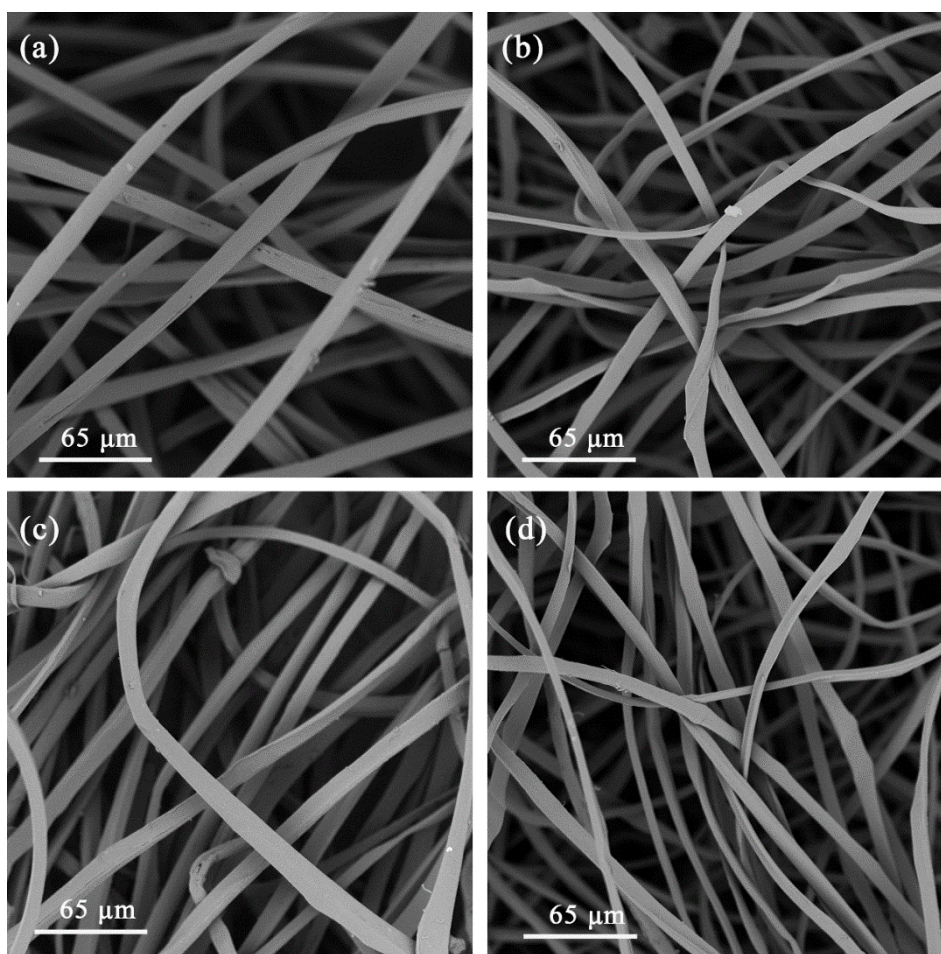
Figure 3-3. SEM images of domestic silk fiber after immersion in various solvents at 80 °C for 24 h: (a) water; (b) DMF; (c) ethanol; and (d) n-hexane.

3.3.2. Verification of the immobilized MOF-76(Tb)

The deposition of MOF-76(Tb) onto the silk fiber was confirmed by XRD patterns of the composite. As shown in Fig. 3-4, the XRD patterns of the composite material synthesized using three different methods (HT, MWA, and LBL) were identical with that of simulated MOF-76(Tb) pattern, suggesting the successful deposition of MOFs material onto the silk fiber surface [92, 93, 125]. The major diffraction peaks associated with MOF-76(Tb) at 11 and 8 degrees were observed in all MOF-76(Tb) coated silk fiber samples [92, 95]. The weakened diffraction peak at 11 degrees was resulted from the combination of simulated MOF-76(Tb) spectrum with the silk fiber pattern. The additional broad diffraction peaks observed between 10 and 30 degrees were associated with the characteristic amorphous diffraction peaks of silk

fiber [124].
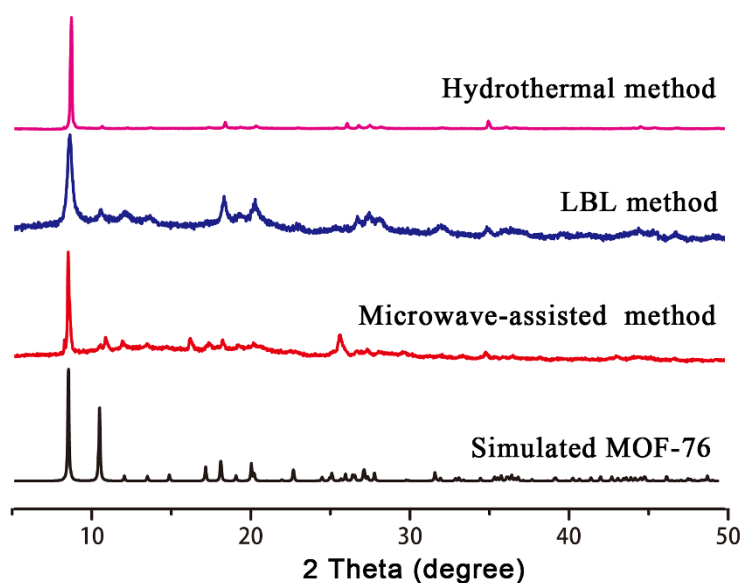
Figure 3-4. XRD patterns of the simulated MOF-76 and MOF-silk fiber composites prepared with three different approaches, i.e. hydro-thermal (HT), layer-by-layer (LBL) and microwave assisted (MWA) methods.

To ensure the full activation of the MOFs coating and bulk MOFs powder, surface area analysis was performed in dynamic vacuum at 120 $^{\circ}$C, which is the heat resistance temperature of the natural silk fiber. However, the surface area value was not measurable, indicating that the pores of the material were not accessible to N_2. This phenomenon is consistent with the previous statement that MOF-76(Tb) does not allow N_2 molecules to enter the pores. It becomes accessible only when the activation temperature is higher than 250 $^{\circ}$C [91, 126, 127]. One noticeable phenomenon is that, after immobilization onto the silk fiber, the reported fluorescence enhancement effect of MOF-76(Tb) was maintained in the case of fluorine ion (Fig. 3-5), revealing no adverse effect of the deposition process on the fluorescent property and the guest molecule diffusion in the channels of MOF-76(Tb). Thus, the deposition of MOF-76(Tb) with the three different methods was successfully achieved with very limited impact on structural strength, surface area or fluorescence property.
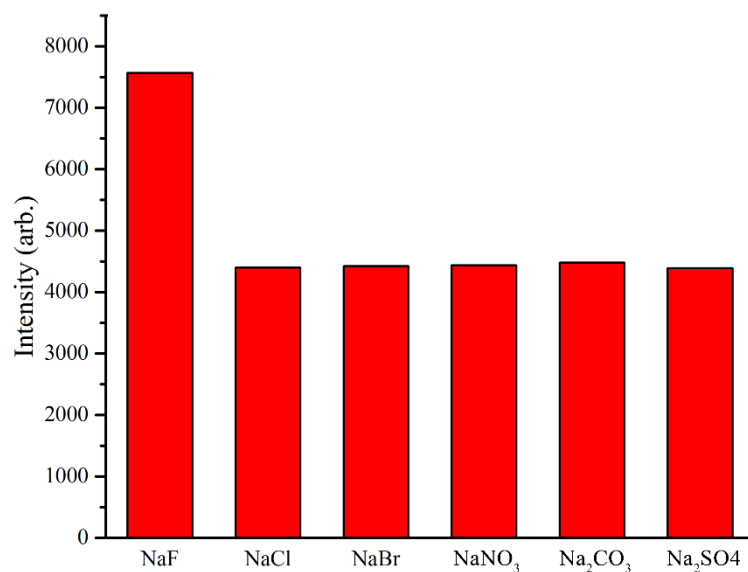
Figure 3-5. Luminescence intensity of the MOF-76-coated silk fiber in 0.5 mM of various ion-containing solutions (at 548 nm).

3.3.3. Pillar-like morphology and poor surface coating via hydrothermal deposition

With the HT method, the immobilized crystals revealed an overall morphology of a cubic column (Fig. 3-6a), which is characteristic of MOF-76(Tb) but about half of the length (40–50 µm) and consequently, half of the weight of conventional MOF-76(Tb) crystals (120 µm, as shown in Fig. 3-7) [94]. Notably, these crystals were perforated by silk fiber, indicating a process of gradual crystal growth on the fiber surface instead of adhering or attaching of the formed crystal to the fiber. According to the theory of self-assembled monolayers (SAMs) [101, 112], the silk fiber was supposed to anchor the Tb^{3+} ions at first and then proceeded with the crystal growth through self-assembly process subsequently.
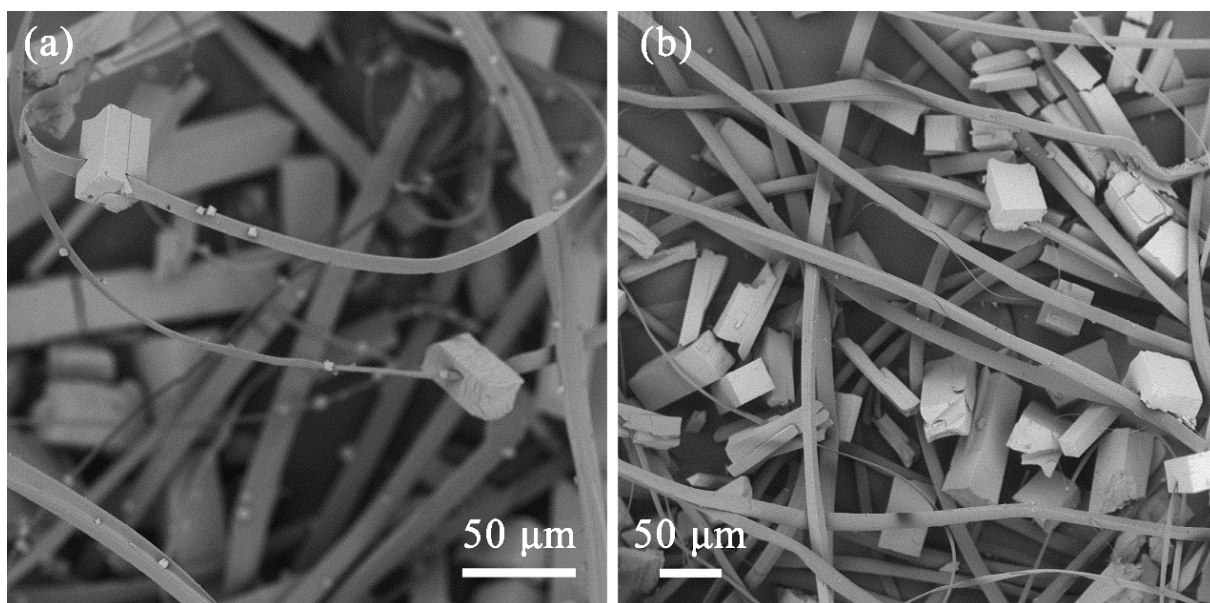
Figure 3-6. SEM images of the MOF-76(Tb)@silk fiber composite prepared by the hydrothermal (HT) method: (a) the immobilized crystals perforated by silk fiber; and (b) the detached crystals entrapped by fiber net.
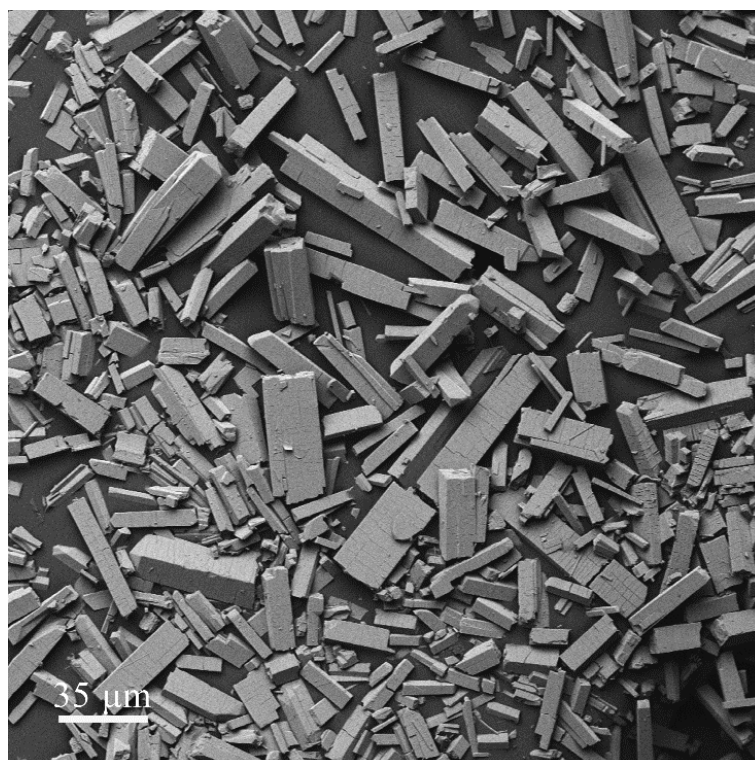
Figure 3-7. SEM image of the MOF-76(Tb) material synthesized with hydrothermal method.

Despite the fact that the fiber surface is rich in functional groups which are conducive to anchoring or coordinating with metal ions and then the formation of MOFs coatings, very few crystals were retained, while a large amount of the normal sized crystals dropped and were entrapped by the fiber net (Fig. 3-6b). Two factors were proposed to bring about this poor coating efficiency. On one hand, inadequate anchoring of Tb^{3+} resulted in limited amount of nucleation sites for the subsequent crystal growth. On the other hand, the formed crystals were detached because of gravity effect. It can be concluded that only those MOFs crystals, having sufficient bonding force (enough nucleation sites) with the silk fiber and limited crystal size (weight), can work against gravity and remain on the surface. In summary, regarding the HT method, low surface coverage and loading rate was obtained, most probably due to the insufficient anchoring of metal precursors and the high detachment rate of normal sized crystals.

3.3.4. Sedimentary-rock-like morphology and improved surface coating via microwave assisted deposition

Under the conditions of the MWA method, which involved soaking at a temperature of 80 °C (at a heating rate of 2 °C/min) for 4 h, a uniform sedimentary-rock-like crystal coverage was obtained (Fig. 3-8a). The crystal size (with a dimension of approximately 10 µm in length and 5 µm in width and thickness) implies an even lighter weight than the pillar-like crystals, agreeing with the previously reported size reduction effect by using microwave or ultrasound method [128, 129]. In addition, the irregular shape of the crystals revealed that the process was performed by successively depositing the crystal flakes under continuous microwave impact. The enhanced microwave disturbance avoided the complete crystal growth, as that accomplished in a static environment, and instead, gave birth to a gradual deposition of crystal flakes. During the self-assembly processes, interactions between the organic and metal precursors created friction between flakes, and between flakes and the fiber, which can compensate for gravity and avoid crystal detaching. Notably, an interesting phenomenon occurred, the crystals prepared with the same method but without silk fiber as substrate retained the conventional pillar-like shape. This can be explained by the isotropy of the synthesis environment. That is, the microwave disturbance effect was minimized in a homogeneous

environment.
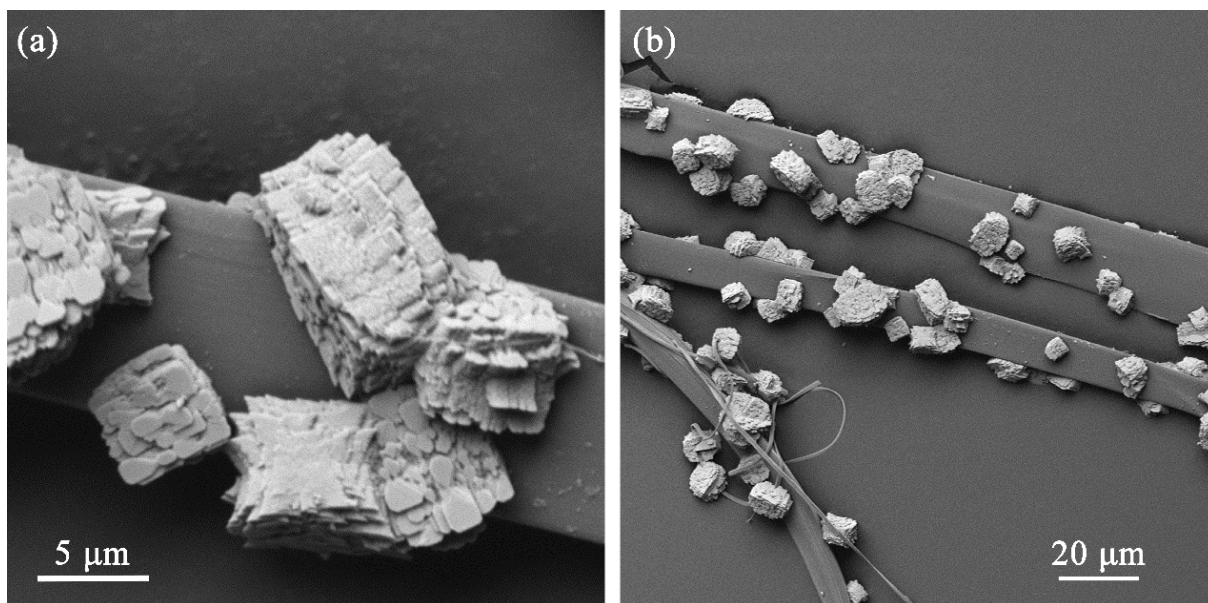
Figure 3-8. SEM images of the MOF-76(Tb)@silk fiber composite prepared by the microwave assisted (MWA) method: (a) the morphology of the immobilized crystals; and (b) the surface coverage of MOF-76(Tb) coating onto the silk fiber.

In addition to the conversion of crystal morphology, an obvious improvement of crystal coverage was realized (Fig. 3-8b), revealing an enhanced process of anchoring Tb^{3+} to form the surface nucleation sites [105]. The higher anchoring efficiency is attributed to the enhanced microwave disturbance which promotes sufficient contact between the fiber and metal ions. To conclude, with the help of microwave disturbance, both increased amount of nucleation sites and limited crystal size/weight were achieved simultaneously, resulting in improved surface coverage and loading rate of MOF-76(Tb).

3.3.5. Needle-like morphology and dense surface coating via LBL deposition

For the composite prepared by the LBL method, the crystal surfaces of the coated MOF-76(Tb) were clearly distinguished (Fig. 3-9), reflecting an overall uniform needle-like morphology and a further controlled crystal size (5~10 µm in length and <1 µm in width). In the above trials, with the HT and MWA methods, the MOF-silk composite still had distinct fiber regions that remained exposed after immobilization of MOF-76. In contrast, by using the

LBL method, the silk fibers could be completely coated with the MOF-76 crystal material. The deposition process was monitored by SEM imaging (Fig. 3-10a-c), which reflected obvious surface coverage improvement after each growth cycle. More importantly, even after being washed several times with ethanol, the coated MOF-76 crystals still remained on the fiber surface, revealing excellent binding force between the crystal and the silk fiber.
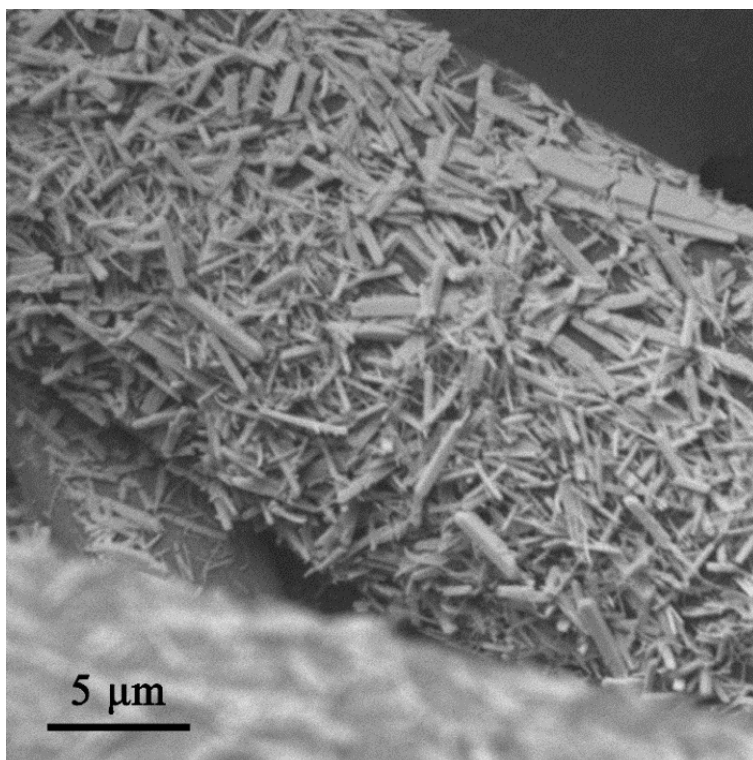
Figure 3-9. SEM image of the MOF-76(Tb)@silk fiber composite prepared by the layer-by-layer (LBL) method.

Besides the limited overall size of the coated MOF-76(Tb) and its needle-like shape, it was found that the crystal size of MOF-76(Tb) formed in the outer layer increased gradually (Figs. 3-10a-c). During each synthesis cycle, a certain amount of the precursor was consumed to form the inner layer of MOF-76(Tb) coating and increase the surface coverage ratio; meanwhile, the rest formed the outer layer coating. With more accessible binding sites supplied by the previously formed inner coating layer, the limiting step of metal ion anchoring for the outer layer formation could be skipped. Accordingly, the crystal size increased rapidly because they could overcome the gravity effect.
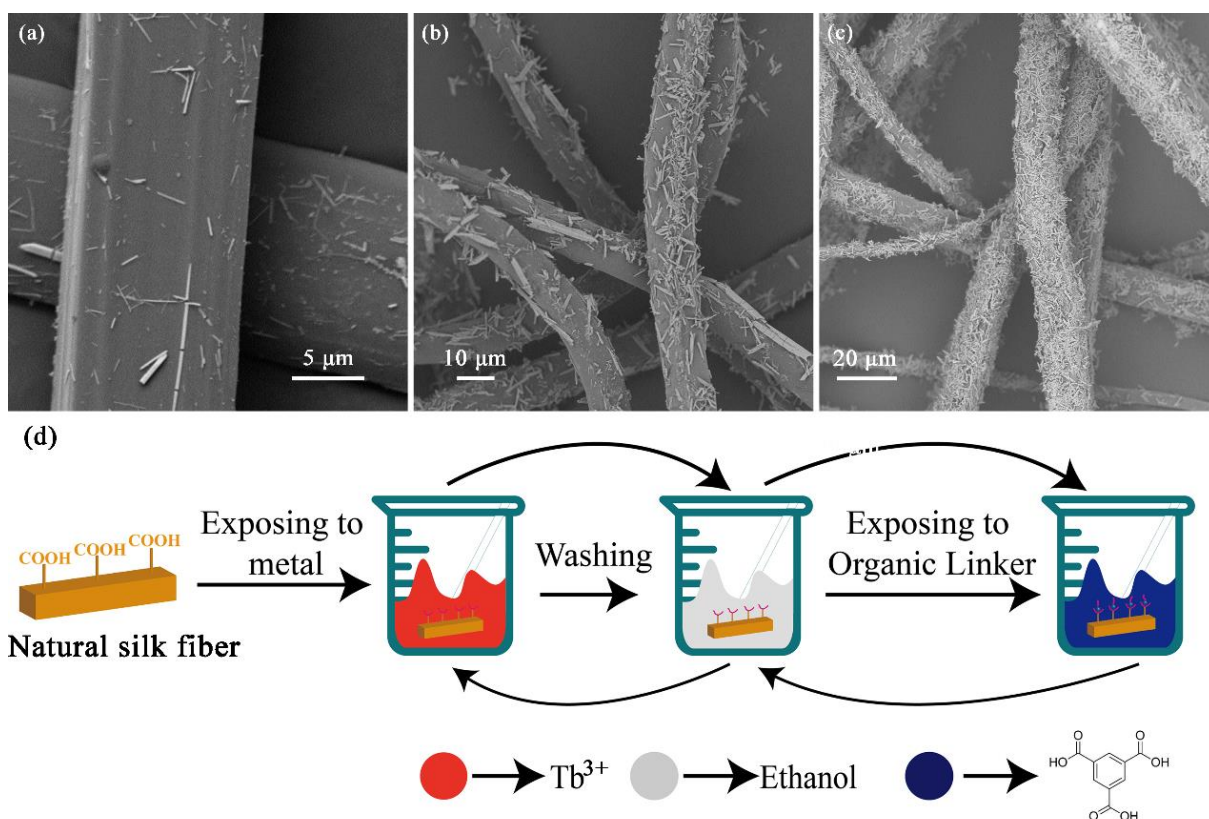
Figure 3-10. SEM images of the MOF-76(Tb) coated silk fibers prepared by the LBL method after the first cycle (a), third cycle (b), and fifth cycle (c), and (d) the schematic of the layer-by-layer (LBL) assembly technique used for the deposition.

For the LBL method, the dramatic increase in surface coverage is most likely associated with the variation in the synthesis procedure. The repeated immersion and cycling in the separated MOF precursor solutions restricted the continuous crystal growth and instead, promoted the anchoring of metal ions through the surface carboxylic groups (Fig. 3-10d) [124]. To conclude, such a high loading efficiency through the LBL method is mainly attributable to the following aspects: (1) the promotion of anchoring metal ions accelerated the full coverage of inner coating layers; (2) the strictly controlled crystal growth prevented the detachment of formed crystals caused by overweight effect; and (3) the formation of multi-coating layers further increased the loading rate. All these aspects were conducive to the dense coating of MOFs layer onto the surface of silk fibers. Compared with the previously reported works using sodium acetate as the capping reagent, the variation in the synthesis procedure is more efficient

in the formation of more nucleation sites and in controlling the crystal size [94, 130, 131].

Taken together, for the immobilization of MOFs onto silk fiber, both the anchoring of Tb^{3+} and the crystal growth play an important role in the preparation process. The former process forms the nucleation sites for surface crystal growth, and the latter determines the detachment ratio of the formed crystals. Among the HT, MW, and LBL methods, varying degrees of anchoring promotion and crystal controlling were achieved, resulting in different coating and loading rates of MOF-76(Tb) onto the natural silk fiber (Table 3-1).

Table 3-1. Contribution of related factors to MOF-76(Tb) coating onto silk fiber

	HT method	MWA method	LBL method
Metal anchoring promotion	✕	√	√ √
Crystal growth control	✕	√	√ √
Coating efficiency	Low	Medium	High

Note: ✕ - little effect, √ - good effect, √ √ - better effect

3.3.6. The composite's potential for colorimetric and fluorescent detection of aquatic Cu^{2+}

An obvious quenching effect of the composite was detected after immersion in 0.5 mM of copper-containing solutions (as shown in Fig. 3-11). The disappearance of typical green fluorescence and a clear change in color from green to grey could be used to make a qualitative judgment in the existence of copper. The intensity of the composite at 548 nm was influenced by cations, especially in the case of Cu^{2+}, showing an obvious selectivity for copper ions (Fig. 3-12). Thus, the silk fibroin-based composite can be proposed for colorimetric sensing of Cu^{2+} in aqueous solution.

K^+ Na^+ Ca^{2+} Al^{3+} Pb^{2+} Ni^{2+} Fe^{3+} Cu^{2+} Cd^{2+}
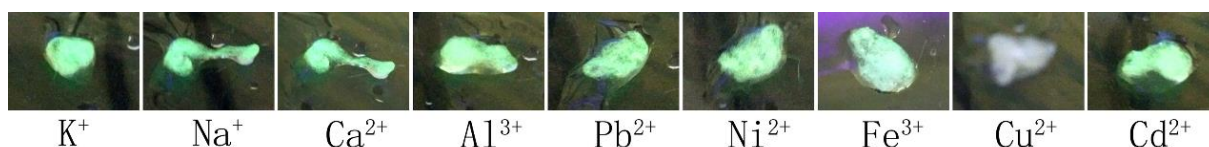
Figure 3-11. Fluorescence images of the MOF-76(Tb)@silk fiber composite after immersion in

equal volumes of solutions containing different metal ions (0.5 mM of M(NO$_3$)$_x$, M = K$^+$, Na$^+$, Al^{3+}, Fe^{3+}, Ca^{2+}, Pb^{2+}, Ni^{2+}, Cd^{2+}, and Cu^{2+}).
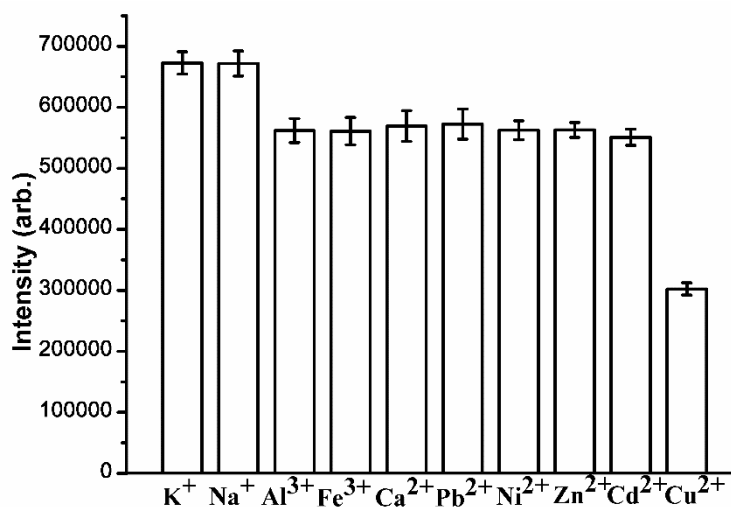
Figure 3-12. Luminescence intensity of the MOF-76(Tb)@silk fiber in 0.5 mM of various cation-containing solutions (at 546 nm).

The recognition of Cu^{2+} might be related with the interaction between Cu^{2+} and the carboxylate oxygen sites on the pore surface of MOF-76(Tb). The interaction between the Cu^{2+} and the benzene-tricarboxylate (BTC) ligands reduced the energy transfer efficiency from BTC to the Tb^{3+} within MOF-76(Tb), thus decreasing the luminescent intensity [132]. Alkali earth cations like Na$^+$ and K$^+$, with saturated electron configuration, almost have no effect on the luminescent intensity [133]. Other divalent and trivalent cations including Ca^{2+}, Pb^{2+}, Zn^{2+}, Cd^{2+}, and Al^{3+} with a close-shell electron configuration, display a light quenching effect due to the weak interaction between Lewis basic sites and metal ions [133, 134]. Although being similar to Cu^{2+}, with an unsaturated electron configuration, Ni^{2+} does not show obvious quenching effect, probably due to the limitation of its ionic radius. In summary, the unique quenching effect for Cu^{2+} possibly resulted from the unsaturated electron configuration and the smaller ionic radius [135].

Initially, the kinetic characteristic for Cu^{2+} detection using the MOF-76@silk fiber composite was tested in this study. Upon the addition of Cu^{2+}, the fluorescence emission

decayed within the initial 5 min and maintained equilibrium subsequently. Therefore, for the following experiments, a reaction time of 5 min was set to ensure the fluorescence equilibrium before measurement. This rapid response is probably brought about by the facile diffusion of Cu^{2+} ions across the porous structure of MOF-76(Tb).
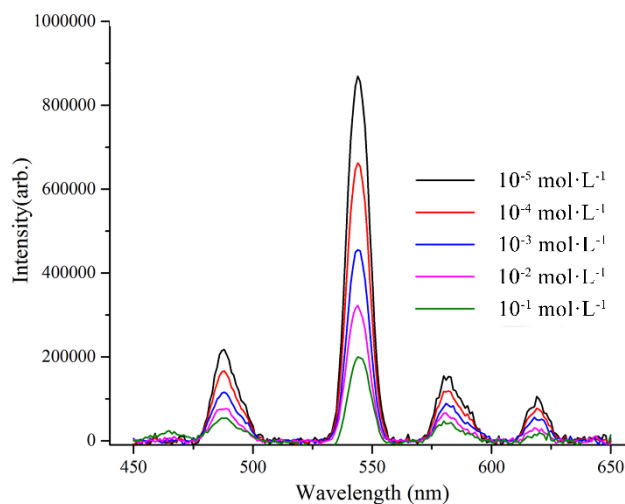
Figure 3-13. PL spectra of the silk fibroin net in aqueous solutions containing different Cu^{2+} concentrations.

Sensitivity is another important factor for evaluating on the performance of the composite material and in the determination on the trace amount of Cu^{2+}. The silk composites were immersed in solutions with gradually increasing Cu^{2+} concentration to further probe its luminescence response property. As shown in Fig. 3-13, the luminescence intensity of the fiber composite was highly sensitive to the Cu^{2+} concentration, and the intensity at 548 nm was almost completely quenched at a concentration of 1×10^{-2} M of Cu^{2+}. The relative luminescence intensity at 548 nm versus the concentration of Cu^{2+} plot showed a decreasing trend, which could be well fitted to a first-order exponential equation ($R^2 = 0.996$, Fig. 3-14), indicating a diffusion-controlled process for its quenching behavior [132, 135]. In addition, a linear fit of I_0/I ratio to copper concentration could be established (Fig. 3-15), reflecting the linear dependence of luminescent quenching on the concentration of Cu^{2+} (i.e., the I_0/I ratio is virtually linearly correlated with the copper concentration within the range of $1\times10^{-3}\sim1\times10^{-5}$ M). Even at a low Cu^{2+} concentration of 0.5 mg/L, the decrease in luminescent intensity was still

detectable. In conclusion, the high selectivity and sensitivity of MOF-76@silk fiber composite makes it a suitable candidate in the application of colorimetric and fluorescent detection of Cu^{2+}.
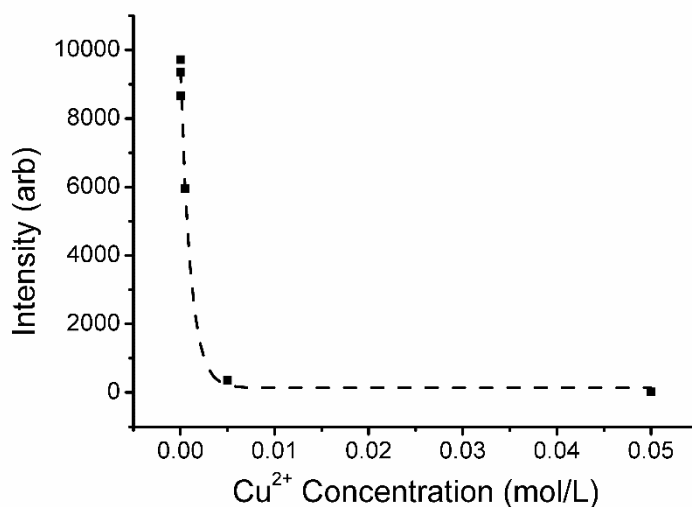
Figure 3-14. Decrease of the luminescence intensity at 548 nm along with the concentration of Cu^{2+}. The dashed line represents an exponential equation fit to the data.

The quenching effect can also be approximately illustrated by the Stern-Volmer equation ($I_0/I = 1 + K_{SV} [M]$). As for the isotherm study, the Stern-Volmer equations under different temperatures are shown in Fig. 3-15. Results showed that the Stern -Volmer quenching constant K_{SV} was negatively correlated with temperature ($K_{SV} = 1192$ or 977 M^{-1}, at 293K or 298K, respectively), indicating that the probable quenching mechanism is static rather than dynamic quenching. This observation is consistent with the speculation that Cu^{2+} might interact with BTC ligand within MOF-76(Tb), resulting in static quenching.
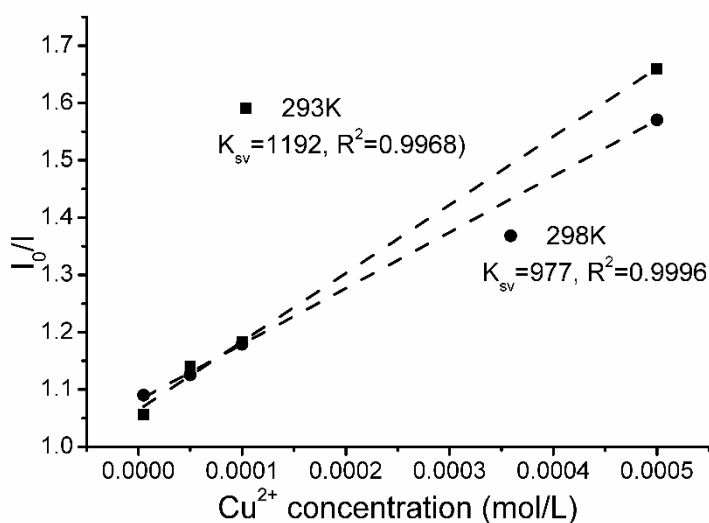
Figure 3-15. Stern-Volmer plots of silk fibroin composite for sensing Cu^{2+} in the range of

$10^{-3} \sim 10^{-5}$ M at different temperatures. The dashed line represents a linear fit to the data.

3.4. Summary

In this work, the domestic silk fiber was utilized as the skeleton for the coating of luminescent MOF-76(Tb). Results show that the silk fiber could be a potential substrate candidate for MOFs coating. Comparing the three synthesis methods (HT, MWA, and LBL) used for MOF-76(Tb) coating, the LBL method could achieve a higher coating efficiency due to the enhanced metal ion anchoring process and the strictly controlled crystal growth. In addition, this new composite could be extended for utilization in colorimetric and fluorescent detection of Cu^{2+} with a low detection limit of 0.5 mg/L. Being different from traditional powdered materials, the MOF-76-coated silk fiber can offer great application potential in real practice because of its convenient usage.

Chapter 4 Synthesis of disposable carbon composite material for cyanide and refractory organics removal from real coking wastewater

4.1 Introduction

Coking wastewater is a typical industrial organic wastewater that characteristically contains high concentrations of contaminants, especially considerable refractory and inhibitory substances such as phenolics and cyanide [136]. In most cases, the effluent chemical oxygen demand (COD) and cyanide concentrations after biological treatment are between 150~300 mg/L and 5.0~15.0 mg/L, respectively. After tertiary treatment, their concentrations can further decrease to COD about 120~200 mg/L and cyanide about 1.5~5.0 mg/L, respectively, which are still higher than the National Integrated Wastewater Discharge Standards (GB8978-1996, COD≤120 mg/L and cyanide ≤ 0.5 mg/L, respectively). This situation is more serious when the new stringent discharge standards specific for coking wastewater (GB16171-2012, COD ≤ 80 mg/L and cyanide ≤ 0.2 mg/L, respectively) is implemented, becoming a bottleneck for the current treatment processes [137]. Thus, more efforts on developing advanced treatment of coking wastewater are still necessary, and special attention should be paid to the enhancement of cyanide and COD removals.

Many trials have been attempted on the tertiary treatment of coking wastewater worldwide. However, conventional chemical oxidation processes cannot completely degrade all the refractory complexes. For instance, the oxidation-reduction potential (ORP) of the Fenton reaction system (600 mV) is invalid for degrading all the refractory complexes. Despite the higher ORP (1.24 V) for chlorine, the essential dosage (6%) has gone far beyond the affordable cost range. Some other newly developed technologies, including electrolytic or ultrasonic oxidation, and wet-air oxidation have only been tested in laboratory, lacking stability and wide adaptability due to their complicated treatment procedures [137-139]. By contrast, adsorption technology is featured with easy operation and high efficiency at low cost, and can thus be used as an effective alternative for the abovementioned technologies.

Polyamidoamine (PAMAM) dendrimers with ethylenediamine core and terminal NH_2-groups are the first class of dendritic polymers to be commercialized [140]. The PAMAM-

modified activated carbon should be the prime candidate for enhanced adsorbent because of being rich in superficial functional groups. Considering that adsorption technology is more suitable for the removal of low concentration of dissolved contaminants [141], coagulation can be implemented as pretreatment to reduce the pollutant load. In this work, a novel powdered activated carbon was prepared by modification with PAMAM, which was then used for the advanced treatment of coking wastewater. COD and cyanide removal efficiencies and the feasibility of integrating adsorption and coagulation technology into one-step treatment process were investigated. Meanwhile, the toxicity of the effluent was tested and the mechanisms involved were discussed. This work is expected to be a feasible and preferable reference for the further treatment of biologically pretreated coking wastewater, especially for its engineering application.

4.2 Materials and methods

4.2.1. Materials

Coking wastewater samples used in this study were collected from the effluent of secondary sedimentation tank in a full-scale treatment plant. The major characteristics of this biologically pretreated coking wastewater were averagely as follows: pH 6.90, COD 156 mg/L, cyanide 6.5 mg/L, and suspended matter about 43 mg/L.

Solid polymeric ferric sulfate (PFS, with iron content > 19%) was purchased from Changlong Technology Co. Ltd, China. Among the typical kinds of activated carbon materials (coconut shell, coal, wood based and so on), the coconut shell activated carbon in powder shape revealed the best treatment performance. Powdered activated carbon (PAC, granularity in 200—300 mesh with methylene blue decolorization rate of 150 mg/g and iodine value of 900 mg/g) used in this study was obtained from Fujian Activated Carbon Co. Ltd, China. PAMAM was obtained from Weihai CY Dendrimer Technology Co. Ltd, China.

The PAMAM-modified powdered activated carbon (MPAC) was prepared with the grafting method [142]. The optimum generation of PAMAM was G2, from which the increased surface functionality and enhanced treatment performance were obtained. Then, the PAC was added into the PAMAM solution (5 wt%) and the suspension was stirred overnight. The final

product was obtained through filtration and drying in a vacuum oven for 24 h.

Table 4-1. The raw wastewater quality

Parameters	Average concentration*	Unit
pH	6.90	-
Suspended matter	43	mg/L
COD_{Cr}	156	mg/L
Ammonia nitrogen	2.03	mg/L
BOD	35.1	mg/L
Total nitrogen	92.3	mg/L
Total phosphorus	0.44	mg/L
Petroleum	0.21	mg/L
Volatile phenols	0.0088	mg/L
Sulfides	0.018	mg/L
Benzene	<0.04	μg/L
Cyanide	6.5	mg/L
Polycyclic aromatic hydrocarbons	0.245	μg/L
Benzo (a) pyrene	<0.0025	μg/L

*Average values of triplicate tests.

4.2.2. Analytical methods

All measurements were performed according to the Standard Methods (APHA, 2005). COD was determined using potassium dichromate as oxidant. Color measurement followed the dilution multiple method. pH value was determined using a pH meter (pHS-3C, Leici, China). Total cyanide was quantified using pyridine-barbituric acid colorimetric method at 580 nm (Hach, DR-4000 UV-Vis spectrophotometer, USA) with a precision of 0.002 mg/L.

4.2.3. Procedures for the treatment process

(1) Bench test

A 20% PFS and 10% MPAC (on weight basis) suspension was prepared using a magnetic stirrer for its stable performance. The optimum dosages of PFS and MPAC were determined by using orthogonal experimental design. The 1L tester filled with water sample was started from rapid mixing at 200 rpm. After 30 s, a certain amount of PFS was added following by mixing at 500 rpm for 2 min for coagulation. Then, a given amount of MPAC was added at 300 rpm for 8 min for reaction. Finally, after 3 min of quiescent settling aided by adding polyacrylamide (PAM), the water samples were taken for water quality measurement. To further investigate the feasibility of adding PFS and MPAC at the same time, a given amount of PFS and MPAC were dissolved and prepared using a magnetic stirrer for its stable performance. The treating efficiencies were evaluated based on COD and cyanide removal efficiencies.

(2) Pilot and industrial tests

The continuous pilot and industrial tests were conducted in one wastewater plant operated by Ma-an-shan Steel Group Co. Ltd, China. The treatment process of the pilot and industrial tests included a grid reaction tank for coagulation and a radial flow sedimentation tank for sedimentation. In these tests, a certain dosage of the mixture solution (containing PFS and MPAC, with the optimum weight ratio based on the bench test) was added and the treatment efficiencies were evaluated based on pollutants removal.

(3) Embryo toxicity assay

Short-term toxicity tests were conducted with zebrafish embryo according to OECD Guideline 212 [143]. Newly fertilized embryos at a same stage of cleavage were collected. The toxicity of final effluent and that with a dilution of 5 times were assayed in triplicate. During the tests, embryos were exposed to the effluent or tested solution under semi-static condition in beaker for four replicates, and the tested solution was renewed every 48 h for nine days. During the exposure, mortality, hatching, and abnormalities of the embryos or larvae were paid more attention, which was daily observed using stereoscopic microscope.

4.3 Results and discussion

4.3.1. Effects of PAC dosage on COD and cyanide removals

Fig. 4-1 shows that both PFS and MPAC dosage exhibit significant influence on COD removal. At a given dosage of PFS, the removal efficiency of COD was continuously increasing with the increase in MPAC dosage, indicating an enhancement effect of adsorption process. In addition to the dosage range shown in Fig. 4-1, the efficiency at higher dosage was also investigated. Results show that the maximum COD removal was achieved at a dosage of 300 mg/L and no significant increase was observed when further increasing MPAC dosage. In this context, 300 mg/L was selected as the upper limit for MPAC dosage in order to control the treatment cost. As for PFS, COD removal performance increased and reached to its maximum (85.3%) at 400 mg/L. A slight decline in COD removal under higher dosage of PFS can be explained by the "re-stabilization" effect.
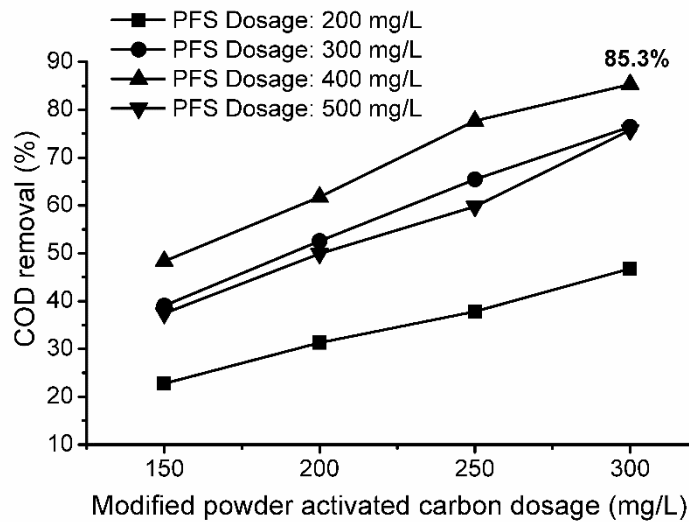
Figure 4-1. Changes in COD removal efficiency under different dosages of modified powder activated carbon (MPAC) at initial COD of 156 mg/L.

Fig. 4-2 shows that generally the cyanide removal efficiency was consistent with COD removal (Fig. 4-1). The optimum dosages of PFS and MPAC are 400 mg/L and 300 mg/L, respectively, achieving the highest cyanide removal of 99.4%. The residual COD (23 mg/L) and cyanide (0.04 mg/L) were much lower than the new discharge standards (COD$\leq$ 80 mg/L and cyanide $\leq$ 0.2 mg/L), indicating that the effluent can be directly discharged with more "margin of safety".
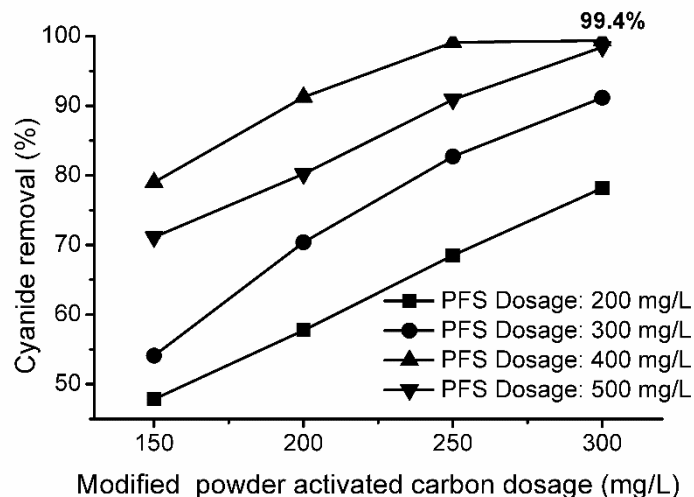
Figure 4-2. Changes in cyanide removal efficiency under different dosages of modified powder activated carbon (MPAC) at initial cyanide of 6.5 mg/L.

4.3.2. Integrated process and its application feasibility

To simplify the operation procedures, the coagulation and adsorption processes were integrated into one-step process, of which the two chemicals were mixed and added at the same time. The feasibility of this integrated process was confirmed by bench scale, pilot, and industrial scale tests (Fig. 4-3), from which good perceptual quality of effluents was obtained. By using this process, the effluent COD decreased from 156 to 29 mg/L with cyanide decreased from 6.5 to 0.06 mg/L, achieving their removal efficiencies at 81.4% and 99.0%, respectively. Despite some slight decline occurred in pollutants removal (85.3% and 99.4% achieved respectively in the former "two-step" process), the integrated "one-step" dosing mode is of great convenience in real practice and the effluent quality can still meet the new discharge standards. It should be noted that the jar test is essential before any application in practice. The dosages of the two chemicals and their ratio are not fixed. Only through jar test can determine the optimum dosage with the treatment cost being controlled.
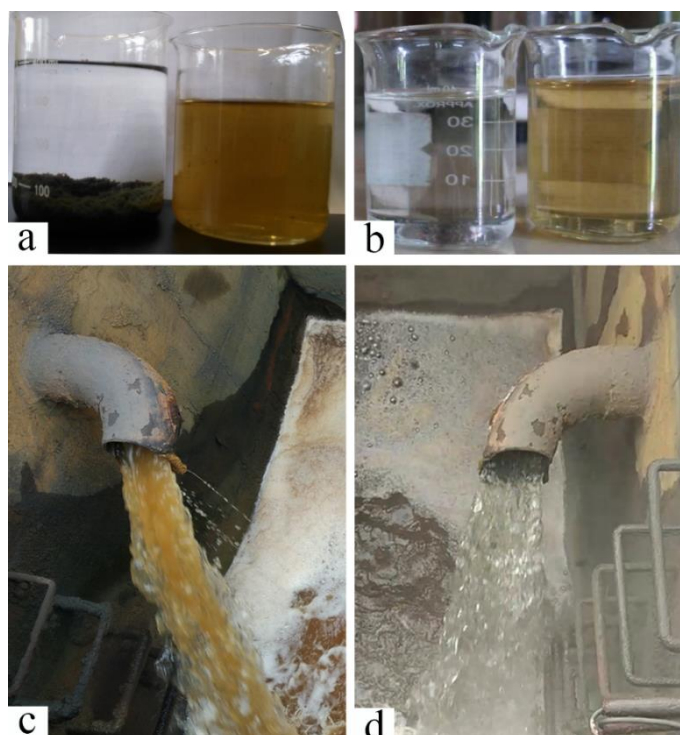
Figure 4-3. Comparison in images between the biologically pretreated coking wastewater and the effluent after the integrated process in bench (a), pilot (b) and industrial tests (c, d).

In addition, the settling efficiency of solid particles in this integrated process improved obviously and the settlement process could be accomplished within 1 min, resulting in large reduction in volume of the sedimentation tank. Besides, the larger flocs size and fractal dimension suggest the compact and solid structure of flocs which are resistant to turbulent flow. When the coking wastewater was treated by this integrated treatment process, the supernatant was further processed by sand filtration. Results showed no significant difference detected in terms of effluent color, COD, and cyanide concentrations, implying that the integrated treatment process is a highly efficient solid-liquid separation process. Thus, no further post-treatment is required for the effluent to meet the discharge standards, reflecting that only one set of coagulation and sedimentation tank is sufficient in real practice, considerably saving investment in infrastructure.

4.3.3. Embryo toxicity assay of the effluent

In Fig. 4-4, the toxicity of the effluents from this integrated process and the factory using

oxidation technology (NaClO, sodium hypochlorite as the oxidant) were conducted and compared on zebrafish embryo or larvae. The hatching rate of the treated water in this study was 47%, whereas the factory effluent (with oxidation technology) was incredibly 0%. Meanwhile, the death rate and abnormal rate of the treated water (20% and 43%, respectively) were lower than those of the NaClO oxidation effluent (27% and 47%, respectively), both demonstrating an obvious improvement in the safety of the treated water.
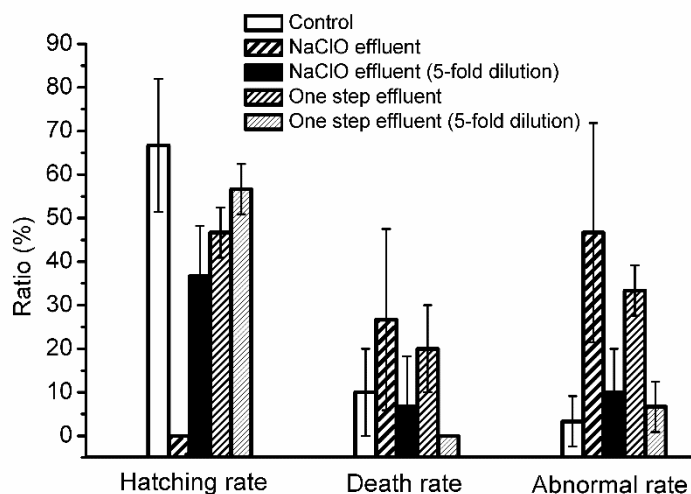
Figure 4-4. Toxicity of coking wastewaters from different tertiary treatment processes on embryo and larvae.

To better simulate the natural dilution process after the effluent being discharged, the toxicity of water samples after fivefold dilution was also attempted in this study. The hatching rate, death rate, and abnormal rate of the treated effluent from the one-step process were 57%, 0%, and 10%, respectively, suggesting that the negative impact of the discharged effluent can be further mitigated during the natural dilution process. In conclusion, the enhanced acute toxicity brought about by conventional oxidation processes (especially under chlorine addition condition) can be avoided by using this integrated physicochemical treatment process [144].

4.3.4. Mechanisms analysis

The insoluble suspended particles and colloidal substances can be removed through the coagulation process with PFS as the coagulant, which effectively reduces the insoluble particle loads in the subsequent treatment processes. In terms of dissolved organic matter in the coking

wastewater, it could be generally fractionated into hydrophobic substances (HOS) and hydrophilic substances (HIS, aniline, phenol, quinoline and isoquinoline) [145, 146]. Among these dissolved organic matters, hydrophobic substances could be removed by adsorption onto the PAC through hydrophobic effect. For hydrophilic substances, they can be adsorbed through the Lewis acid-base interactions: the PAMAM dendrimer coated onto the surface of the PAC has a certain strength of Lewis base and can thus form Lewis acid-base interaction with the excessive linear macromolecule of poly-ferric. This means that the dendrimer and poly-ferric could be combined into a new Lewis acid system to further promote reaction with the hydrophilic substances (with the nature of Lewis base) and realize the enrichment and removal of hydrophilic organic pollutants consequently. As for cyanide, the mechanisms involved are similar with those of hydrophilic organic substances: the dendrimer and poly-ferric are firstly combined into a positively charged system through Lewis acid-base interaction; then cyanide could be adsorbed onto the surface through electrostatic interaction; after the followed-up settling process, these negatively charged pollutants can be removed finally.

An obviously synergistic effect was observed between the coagulation and adsorption processes, because the treatment performance of this integrated process (85.3%) is much higher than the sum of single coagulation (17.1% at PFS dosage of 400 mg/L) and single adsorption (27.4% at MPAC dosage of 300 mg/L). The link between coagulation and adsorption includes two aspects. Firstly, the dendrimer coated onto the surface of activated carbon and the excessive poly-ferric formed a new Lewis acid system to promote enrichment of hydrophilic substances and cyanide compound. Then, the settling efficiency of flocs in this integrated process improved obviously. The reasons can be explained as follows. On the one hand, PAC can function as the coagulation kernel to initial and assist the coagulation process. On the other hand, the PAMAM dendrimer coated on the activated carbon can enhance the bridge formation and catching-sweeping effect in the flocculation process (Fig. 4-5).
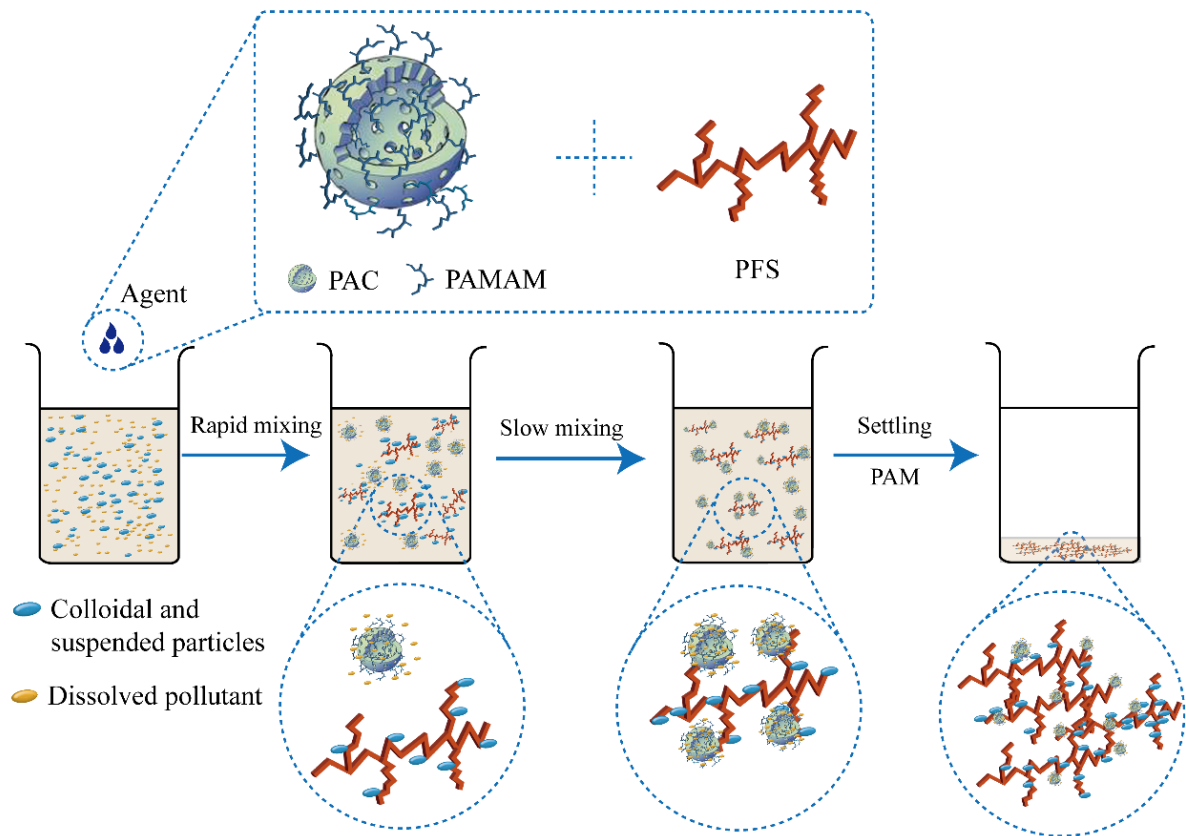
Figure 4-5. Proposed mechanisms for the integrated process and simulated locations of suspended and dissolved particles onto PFS and MPAC, respectively.

4.4 Summary

A novel integrated treatment process was developed for the advanced treatment of biologically pretreated coking wastewater. The maximum COD and cyanide removals were 85.3% and 99.4%, respectively, possibly attributable to the synergistic effect of coagulation and adsorption processes. Thus, this novel process with high efficiency, easy operation, and lower environmental impact can serve as a potential technology for the advanced treatment of coking wastewater. It should be noted that currently MPAC is not a commercialized product, thus the capital investment might be a little bit higher, which needs to be carefully considered before its engineering application in practice.

Chapter 5 Conclusions and further research

5.1 Conclusions

This thesis is devoted to promote the scaling up application of adsorption-based technology for aquatic inorganic contaminants removal/detection. Efforts were made to overcome the common problem of efficiency gap between the laboratory research and the real practice, and the inconvenience nature of most powdered adsorbent materials in application.

In laboratory bench scale research, a more practical and comprehensive evaluation system should be put forward, which gives full consideration of material's adaptability to water environment (pollutant concentration, pH, coexisting ions), adsorption rate, and regeneration capacity. In this context, ZIF-8 (a typical kind of water stable porous material prepared in Chapter 2 of this study) outperformed other materials and, thus, revealed great application potential for arsenate removal, especially for trace arsenate (ppb, μg/L) in drinking water (shown in Fig. 5-1). Conclusions regarding the arsemate removal efficiency and the mechanism can be drawn as follows:

(1) ZIF-8 owned the first and highest reported adsorption capacity (76.5 mg/g) at a low equilibrium concentration (9.8 μg/L).

(2) Satisfactory adsorption properties (higher adsorption capacity, faster adsorption rate, adaptability to water environment, and good regeneration capacity) demonstrated the feasibility of using ZIF-8 as an efficient adsorbent for the removal of aquatic trace arsenate.

(3) Production of large amounts of external active sites (Zn-OH) through the dissociative adsorption of water and subsequent formation of an inner-sphere complex with arsenate molecule are the proposed mechanisms involved in As(V) adsorption onto ZIF-8 surface.
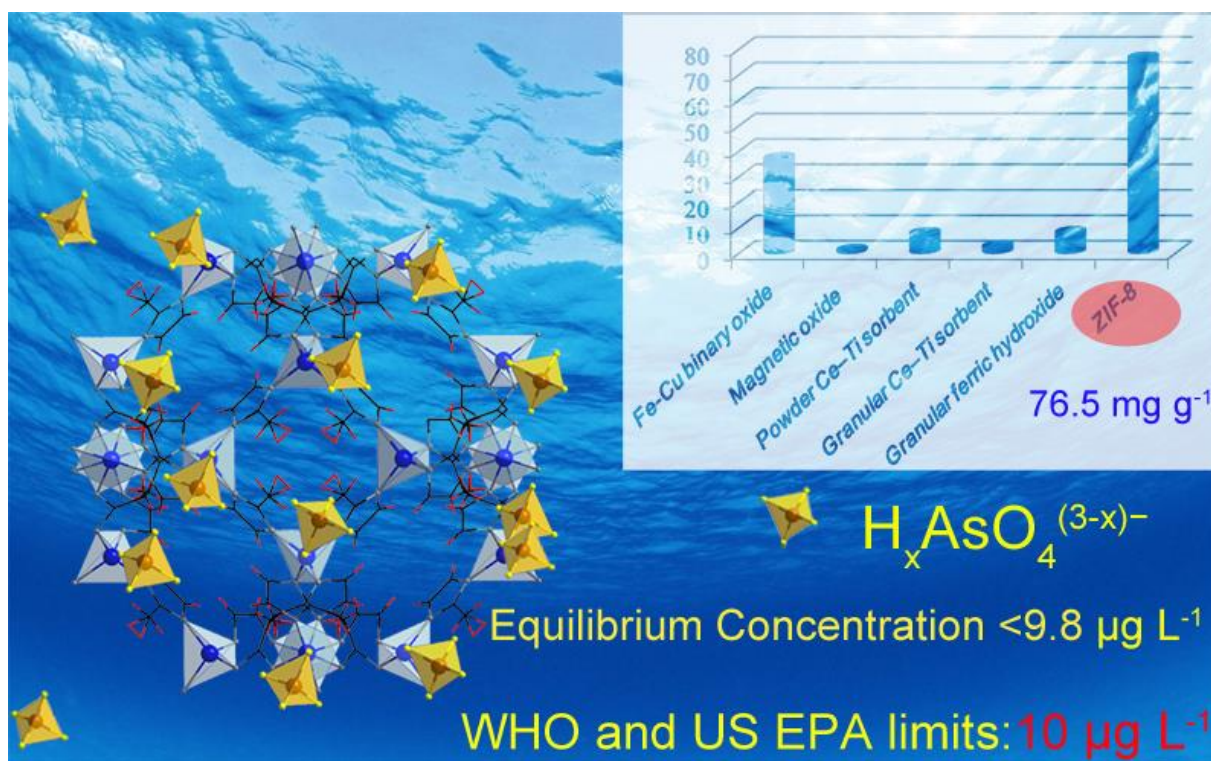
Figure 5-1. High efficiency of ZIF-8 for adsorption removal of trace arsenate in drinking water.

When it comes to the semi-industrial test or business application stage, another important issue is to realize the easy solid-liquid separation and prevent the weight loss of powdered material in real practice. In Chapter 3 of this study, domestic silk fiber was applied as the skeleton, and layer-by-layer (LBL) strategy was used as the deposition method, which changed the form of MOF-76(Tb) from powder to cloth and thus brought great usage convenience (as shown in Fig. 5-2). In addition, the fluorescent property of the raw material was maintained, implying limited functional impact of the deposition process. In this context, the application of nature silk fiber as substrate and LBL method as the coating process could serve as a novel strategy for preparing composite material and realizing easier solid-liquid separation. Conclusions can be drawn as follows:

(1) The silk fiber is a good substrate candidate for MOF-76 coating owning to its abundant surface carboxylic groups and solvent resistance.

(2) Among the three typical preparation methods, i.e. hydro-thermal (HT), microwave assisted (MWA), and layer-by-layer (LBL), LBL was found to be the optimum method for the

deposition of MOF-76, due to the enhanced metal ion anchoring process and the strictly controlled crystal growth.

(3) High selectivity and sensitivity for copper detection were attained in the fiber net composite (a linear detection concentration range of $10^{-3} \sim 10^{-5}$ M and a low detection limit up to 0.5 mg/L).
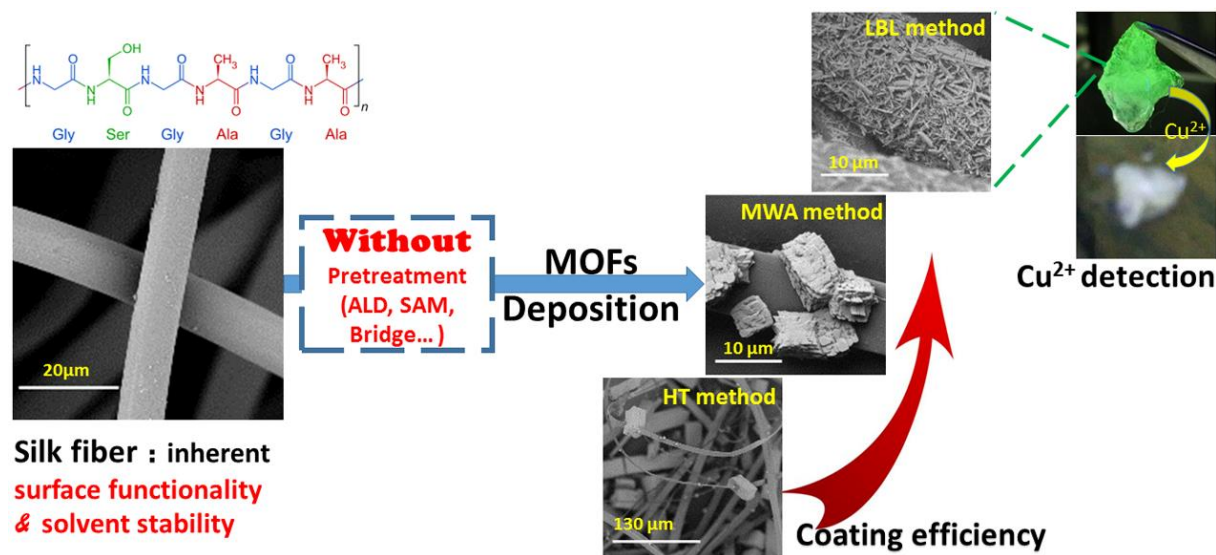
Figure 5-2. Deposition of MOF-76(Tb) onto natural silk fiber for feasible copper detection.

An alternative strategy for the immobilization of powdered material onto other substrates is to develop disposable materials, which can be discharged after usage and avoid the process of materials recovery. In Chapter 4 of this study, through modification of powdered activated carbon with polyamidoamine (PAMAM) and integrating adsorption and coagulation processes, a novel composite material was newly developed, which revealed high efficiency for cyanide and refractory organics removal from real coking wastewater (Fig. 5-3). The composite's high removal efficiency, lower cost, and usage convenience ('reaction-discharging' mode) reflect its great engineering application potential in wastewater treatment practice, and open up a new path to apply adsorption-based technology for wastewater treatment. The following conclusions can be arrived at from this work:

(1) Results of laboratory, pilot, and industrial-scale experiments indicated that this novel composite material can remove bio-refractory pollutants, achieving the maximum chemical oxygen demand (COD) and cyanide removals of around 85.3% and 99.4%, respectively.

(2) The effluent could meet the corresponding discharge standards without any further treatment, i.e., COD < 30 mg/L, cyanide < 0.1 mg/L, and improved effluent safety (lower toxicity).

(3) The usage convenience and high efficiency of this composite material reflect its application potential in the actual tertiary treatment of coking wastewater.
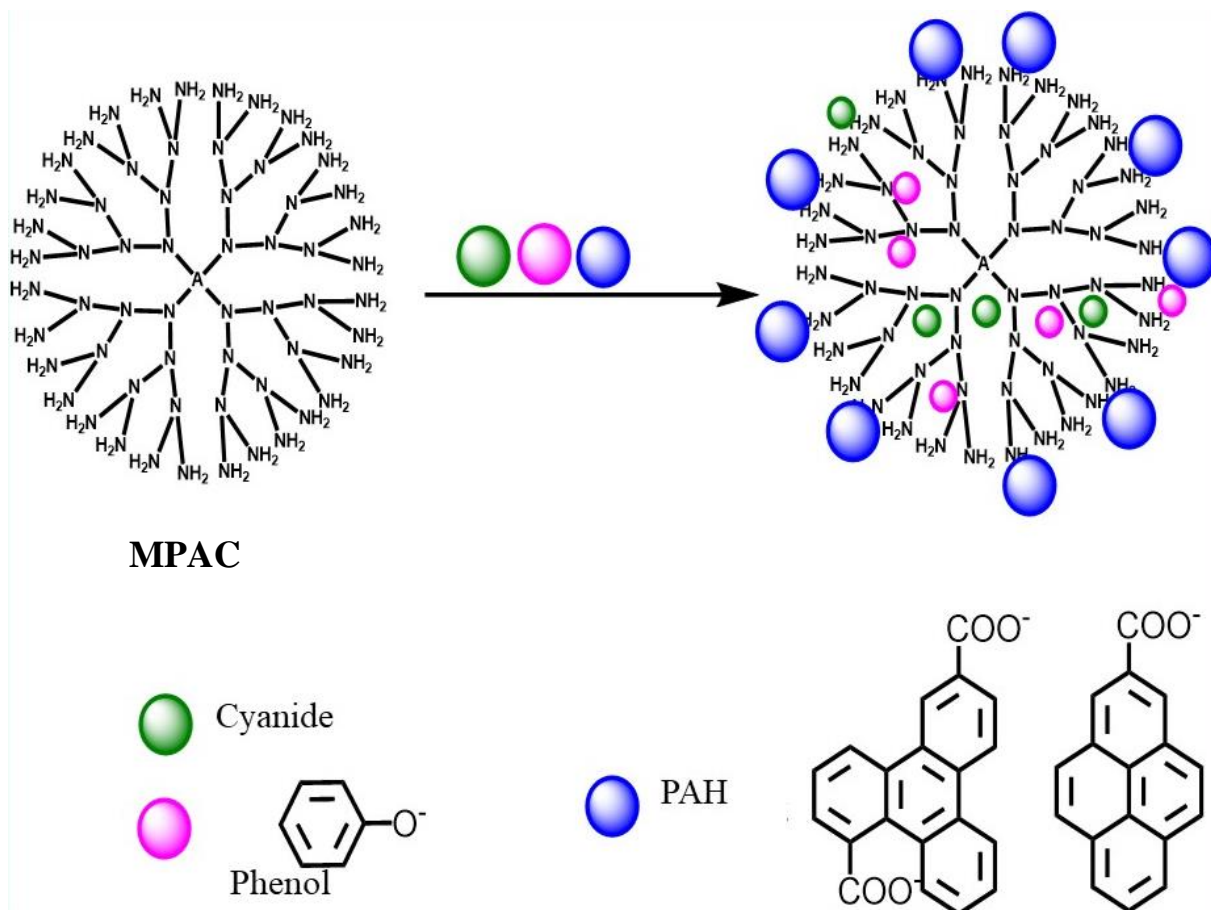
Figure 5-3. Simulated location of various pollutants in the modified activated carbon (MPAC) material.

Results from this work are expected to shed light on the related research and contribute to better application of adsorption-based technology in the real practice of water treatment and water quality monitoring.

5.2 Further research plan

To make full use of the adsorption based technology in practical water and wastewater treatment, future research should be followed up in several aspects:

(1) The preparation cost is a key factor that restricts the application of some newly developed adsorbent materials or chemicals. Either for ZIF-8, MOF-76, or the PAMAM agent, more efforts should be made on the development of new synthesis strategy with lower cost.

(2) For the application of ZIF-8 in chapter 2, column study needs to be conducted to fully evaluate the treating efficiency of the newly developed adsorbent material.

(3) For the deposition of MOF-76(Tb) onto silk fibers in chapter 3, the feasibility of the LBL method for the preparation of other MOFs composite as a tissue material needs to be investigated.

(4) For the development of highly efficient and disposable adsorbent in chapter 4, the feasibility of integrating the coagulant, adsorbent, and modification agents into a final form of chemicals should be investigated, which will greatly simplify the on-site operation and management of wastewater plant.

References

[1] M.M. Pendergast, E.M.V. Hoek, A review of water treatment membrane nanotechnologies, *Energy. Environ. Sci.* 4 (2011) 1946-1971.

[2] Y. Zhang, B. Wu, H. Xu, H. Liu, M. Wang, Y. He, B. Pan, Nanomaterials-enabled water and wastewater treatment, *NanoImpact* 3-4 (2016) 22-39.

[3] J. Alcamo, T. Henrichs, T. Rösch, World Water in 2025: Global Modeling and Scenario Analysis for the World Commission on Water for the 21st Century, kassel world water series 2, center for environmental systems research, University of Kassel, Germany (2017).

[4] M.M. Mekonnen, A.Y. Hoekstra, Four billion people facing severe water scarcity, *Sci. Adv.* 2 (2016) e1500323.

[5] UN WWAP, 2009. United Nations World Water Assessment Programme, The World Water Development Report 3: Water in a Changing World. UNESCO, Paris, France (2016).

[6] Ministry of Environmental Protection of the People's Republic of China (MEPPRC), China Environmental State Bulletin, Beingjing, China (2016).

[7] R.P. Schwarzenbach, B.I. Escher, K. Fenner, T.B. Hofstetter, C.A. Johnson, U. Von Gunten, B. Wehrli, The challenge of micropollutants in aquatic systems, *Science* 313 (2006) 1072-1077.

[8] J.O. Nriagu, J.M. Pacyna, Quantitative assessment of worldwide contamination of air, water and soils by trace metals, *Nature* 333 (1988) 134-139.

[9] F.X. Han, A. Banin, Y. Su, D.L. Monts, M.J. Plodinec, W.L. Kingery, G.E. Triplett, Industrial age anthropogenic inputs of heavy metals into the pedosphere, *Naturwissenschaften* 89 (2002) 497-504.

[10] R.S. Boyd, Heavy metal pollutants and chemical ecology: exploring new frontiers, *J. Chem. Ecol.* 36 (2010) 46-58.

[11] R.P. Schwarzenbach, T. Egli, T.B. Hofstetter, U. von Gunten, B. Wehrli, Global water pollution and human health, *Annu. Rev. Environ. Resour.* 35 (2010) 109-136.

[12] I. Douglas, N. Lawson, Material Flows Due to Mining and Urbanization, In: A Handbook

of Industrial Ecology, Edward Elgar Publishing Limited, France (2002).

[13] G. Bridge, Contested terrain: mining and the environment, *Annu. Rev. Environ. Resour.* 29 (2004) 205-259.

[14] R.R. Dash, A. Gaur, C. Balomajumder, Cyanide in industrial wastewaters and its removal: a review on biotreatment, *J. Hazard. Mater.* 163 (2009) 1-11.

[15] D.K. Nordstrom, Worldwide occurrences of arsenic in ground water, *Science* 296 (2002) 2143-2145.

[16] M. Amini, K.C. Abbaspour, M. Berg, L. Winkel, S.J. Hug, E. Hoehn, H. Yang, C.A. Johnson, Statistical modeling of global geogenic arsenic contamination in groundwater, *Environ. Sci. Technol.* 42 (2008) 3669-3675.

[17] M. Amini, K. Mueller, K.C. Abbaspour, T. Rosenberg, M. Afyuni, K.N. Møller, M. Sarr, C.A. Johnson, Statistical modeling of global geogenic fluoride contamination in groundwaters, *Environ. Sci. Technol.* 42 (2008) 3662-3668.

[18] P. Smedley, D. Kinniburgh, A review of the source, behaviour and distribution of arsenic in natural waters, *Appl. Geochem.* 17 (2002) 517-568.

[19] A.A. Duker, E. Carranza, M. Hale, Arsenic geochemistry and health, *Environ. Inter.* 31 (2005) 631-641.

[20] S. Murcott, Arsenic Contamination in The World, IWA publishing, London, UK (2012).

[21] L. Rodríguez-Lado, G. Sun, M. Berg, Q. Zhang, H. Xue, Q. Zheng, C.A. Johnson, Groundwater arsenic contamination throughout China, *Science* 341 (2013) 866-868.

[22] V.K. Sharma, M. Sohn, Aquatic arsenic: toxicity, speciation, transformations, and remediation, *Environ. Inter.* 35 (2009) 743-759.

[23] V.K. Gupta, I. Ali, T.A. Saleh, A. Nayak, S. Agarwal, Chemical treatment technologies for waste-water recycling-an overview, *RSC Adv.* 2 (2012) 6380.

[24] M. Bilal, J.A. Shah, T. Ashfaq, S.M. Gardazi, A.A. Tahir, A. Pervez, H. Haroon, Q. Mahmood, Waste biomass adsorbents for copper removal from industrial wastewater-a review, *J. Hazard. Mater.* 263(2) (2013) 322-333.

[25] M.A. Hashim, S. Mukhopadhyay, J.N. Sahu, B. Sengupta, Remediation technologies for

heavy metal contaminated groundwater, *J. Environ. Manage.* 92 (2011) 2355-2388.

[26] C.A. Johnson, The fate of cyanide in leach wastes at gold mines: An environmental perspective, *Appl. Geochem.* 57 (2015) 194-205.

[27] F. Bhunia, N. Saha, A. Kaviraj, Toxicity of thiocyanate to fish, plankton, worm, and aquatic ecosystem, *B. Environ. Contam. Tox.* 64 (2000) 197-204.

[28] J. Liu, J. He, Y. Yuan, J. Zhang, Effects of different coagulants on flocculation performance and floc properties in northwest China raw water treatment, *Water Sci. Tech-W. Sup.* 15 (2015) 599-605.

[29] A. Matilainen, M. Vepsäläinen, M. Sillanpää, Natural organic matter removal by coagulation during drinking water treatment: a review, *Adv. Colloid. Interfac.* 159 (2010) 189-197.

[30] Q. Chang, G. Wang, Study on the macromolecular coagulant PEX which traps heavy metals, *Chem. Eng. Sci.* 62 (2007) 4636-4643.

[31] M. Huerta-Fontela, M.T. Galceran, F. Ventura, Occurrence and removal of pharmaceuticals and hormones through drinking water treatment, *Water Res.* 45 (2011) 1432-1442.

[32] N. Le-Minh, S. Khan, J. Drewes, R. Stuetz, Fate of antibiotics during municipal water recycling treatment processes, *Water Res.* 44 (2010) 4295-4323.

[33] T. Peters, Membrane Technology for Water Treatment, *Chem. Eng. Technol.* 33 (2010) 1233-1240.

[34] F. Fu, Q. Wang, Removal of heavy metal ions from wastewaters: a review, *J. Environ. Manage.* 92 (2011) 407-418.

[35] D. Lakherwal, Adsorption of heavy metals: a review, *Inter. J. Environ. Res. Dev.* 4 (2014) 41-48.

[36] J.-S. Kwon, S.-T. Yun, J.-H. Lee, S.-O. Kim, H.Y. Jo, Removal of divalent heavy metals (Cd, Cu, Pb, and Zn) and arsenic(III) from aqueous solutions using scoria: kinetics and equilibria of sorption, *J. Hazard. Mater.* 174 (2010) 307-313.

[37] G. Ramakrishna, M. Susmita, Application of response surface methodology for

optimization of Cr(III) and Cr(VI) adsorption on commercial activated carbons, *J. Chem. Sci.* 2231 (2012) 606X.

[38] A. Bhatnagar, W. Hogland, M. Marques, M. Sillanpää, An overview of the modification methods of activated carbon for its water treatment applications, *Chem. Eng. J.* 219 (2013) 499-511.

[39] C. Huang, L.M. Vane, Enhancing removal by a activated carbon, *Res. J. Water Pollut. C.* (1989) 1596-1603.

[40] W. Chen, R. Parette, J. Zou, F.S. Cannon, B.A. Dempsey, Arsenic removal by iron-modified activated carbon, *Water Res.* 41 (2007) 1851-1858.

[41] Q. Chang, W. Lin, W.C. Ying, Preparation of iron-impregnated granular activated carbon for arsenic removal from drinking water, *J. Hazard. Mater.* 184 (2010) 515-522.

[42] A.V. Vitela-Rodriguez, J.R. Rangel-Mendez, Arsenic removal by modified activated carbons with iron hydro(oxide) nanoparticles, *J. Environ. Manage.* 114 (2013) 225-231.

[43] C. Nieto-Delgado, J.R. Rangel-Mendez, Anchorage of iron hydro(oxide) nanoparticles onto activated carbon to remove As(V) from water, *Water Res.* 46 (2012) 2973-2982.

[44] P. Mondal, C. Balomajumder, B. Mohanty, A laboratory study for the treatment of arsenic, iron, and manganese bearing ground water using Fe^{3+} impregnated activated carbon: effects of shaking time, pH and temperature, *J. Hazard. Mater.* 144 (2007) 420-426.

[45] V. Strelko, Jr., D.J. Malik, Characterization and metal sorptive properties of oxidized active carbon, *J. Colloid. Interface. Sci.* 250 (2002) 213-220.

[46] J.-K. Yang, H.-J. Park, H.-D. Lee, S.-M. Lee, Removal of Cu(II) by activated carbon impregnated with iron(III), *Colloid. Surface. A* 337 (2009) 154-158.

[47] N. Adhoum, L. Monser, Removal of cyanide from aqueous solution using impregnated activated carbon, *Chem. Eng. Process.* 41 (2002) 17-21.

[48] M. Khajeh, S. Laurent, K. Dastafkan, Nanoadsorbents: classification, preparation, and applications (with emphasis on aqueous media), *Chem. Rev.* 113 (2013) 7728-7768.

[49] N.A. Khan, Z. Hasan, S.H. Jhung, Adsorptive removal of hazardous materials using metal-organic frameworks (MOFs): a review, *J. Hazard. Mater.* 244-245 (2013) 444-456.

[50] H. Li, M. Eddaoudi, M. O'Keeffe, O.M. Yaghi, Design and synthesis of an exceptionally stable and highly porous metal-organic framework, *Nature* 402 (1999) 276-279.

[51] D. Mohan, C.U. Pittman, Jr., Arsenic removal from water/wastewater using adsorbents-a critical review, *J. Hazard. Mater.* 142 (2007) 1-53.

[52] T.S.Y. Choong, T.G. Chuah, Y. Robiah, F.L. Gregory Koay, I. Azni, Arsenic toxicity, health hazards and removal techniques from water: an overview, *Desalination* 217 (2007) 139-166.

[53] J.L.C. Rowsell, O.M. Yaghi, Metal–organic frameworks: a new class of porous materials, *Micropor. Mesopor. Mater.* 73 (2004) 3-14.

[54] K.S. Park, Z. Ni, A.P. Cote, J.Y. Choi, R. Huang, F.J. Uribe-Romo, H.K. Chae, M. O'Keeffe, O.M. Yaghi, Exceptional chemical and thermal stability of zeolitic imidazolate frameworks, *Proc. Natl. Acad. Sci. USA* 103 (2006) 10186-10191.

[55] Z. Zhang, S. Xian, H. Xi, H. Wang, Z. Li, Improvement of CO_2 adsorption on ZIF-8 crystals modified by enhancing basicity of surface, *Chem. Eng. Sci.* 66 (2011) 4878-4888.

[56] Y.N. Wu, M. Zhou, B. Zhang, B. Wu, J. Li, J. Qiao, X. Guan, F. Li, Amino acid assisted templating synthesis of hierarchical zeolitic imidazolate framework-8 for efficient arsenate removal, *Nanoscale* 6 (2014) 1105-1112.

[57] B. Van de Voorde, B. Bueken, J. Denayer, D. De Vos, Adsorptive separation on metal-organic frameworks in the liquid phase, *Chem. Soc. Rev.* 43 (2014) 5766-5788.

[58] L. Zhang, G. Wu, J. Jiang, Adsorption and Diffusion of CO_2 and CH_4 in zeolitic imidazolate framework-8: effect of structural flexibility, *J. Phys. Chem. C* 118 (2014) 8788-8794.

[59] K. Zhang, A. Nalaparaju, Y. Chen, J. Jiang, Biofuel purification in zeolitic imidazolate frameworks: the significant role of functional groups, *Phys. Chem. Chem. Phys.* 16 (2014) 9643-9655.

[60] J.Q. Jiang, C.X. Yang, X.P. Yan, Zeolitic imidazolate framework-8 for fast adsorption and removal of benzotriazoles from aqueous solution, *ACS Appl. Mater. Inter.* 5 (2013) 9837-9842.

[61] P. Ghosh, K.C. Kim, R.Q. Snurr, Modeling water and ammonia adsorption in hydrophobic metal-organic frameworks: single components and mixtures, *J. Phys. Chem. C* 118 (2014) 1102-1110.

[62] A.U. Ortiz, A.P. Freitas, A. Boutin, A.H. Fuchs, F.X. Coudert, What makes zeolitic imidazolate frameworks hydrophobic or hydrophilic? The impact of geometry and functionalization on water adsorption, *Phys. Chem. Chem. Phys.* 16 (2014) 9940-9949.

[63] C.l. Chizallet, S. Lazare, D. Bazer-Bachi, F. Bonnier, V. Lecocq, E. Soyer, A.-A. Quoineaud, N. Bats, Catalysis of transesterification by a nonfunctionalized metal-organic framework: acido-basicity at the external surface of ZIF-8 probed by FTIR and ab initio calculations, *J. Am. Chem. Soc.* 132 (2010) 12365-12377.

[64] C. Chizallet, N. Bats, External surface of zeolite imidazolate frameworks viewed sb initio: multifunctionality at the organic-inorganic interface, *J. Phys. Chem. Lett.* 1 (2009) 349-353.

[65] K. Zhang, R.P. Lively, C. Zhang, W.J. Koros, R.R. Chance, Investigating the intrinsic ethanol/water separation capability of ZIF-8: an adsorption and diffusion study, *J. Phys. Chem. C* 117 (2013) 7214-7225.

[66] L.B. Sun, J.R. Li, J. Park, H.C. Zhou, Cooperative template-directed assembly of mesoporous metal-organic frameworks, *J. Am. Chem. Soc.* 134 (2012) 126-129.

[67] Y. Pan, Y. Liu, G. Zeng, L. Zhao, Z. Lai, Rapid synthesis of zeolitic imidazolate framework-8 (ZIF-8) nanocrystals in an aqueous system, *Chem. Commun.* 47 (2011) 2071-2073.

[68] J. Cravillon, S. Münzer, S.-J. Lohmeier, A. Feldhoff, K. Huber, M. Wiebcke, Rapid room-temperature synthesis and characterization of nanocrystals of a prototypical zeolitic imidazolate framework, *Chem. Mater.* 21 (2009) 1410-1412.

[69] P. Tan, J.-X. Qin, X.-Q. Liu, X.-Q. Yin, L.-B. Sun, Fabrication of magnetically responsive core-shell adsorbents for thiophene capture: AgNO$_3$-functionalized Fe$_3$O$_4$@mesoporous SiO$_2$ microspheres, *J. Mater. Chem. A* 2 (2014) 4698-4705.

[70] X. Dou, D. Mohan, C.U. Pittman, Jr., Arsenate adsorption on three types of granular

schwertmannite, *Water Res.* 47 (2013) 2938-2948.

[71] Z. Li, S. D, G.Y, J. H, V. C. Lim., As(V) and As(III) removal from water by a Ce-Ti oxide adsorbent:Behavior and mechanism, *Chem. Eng. J.* 161 (2010) 106-113.

[72] C.T. Yavuz, J.T. Mayo, W.W. Yu, A. Prakash, J.C. Falkner, S. Yean, L. Cong, H.J. Shipley, A. Kan, M. Tomson, D. Natelson, V.L. Colvin, Low-field magnetic separation of monodisperse Fe_3O_4 nanocrystals, *Science* 314 (2006) 964-967.

[73] G. Zhang, Z. Ren, X. Zhang, J. Chen, Nanostructured iron(III)-copper(II) binary oxide: a novel adsorbent for enhanced arsenic removal from aqueous solutions, *Water Res.* 47 (2013) 4022-4031.

[74] M. Badruzzaman, P. Westerhoff, D.R. Knappe, Intraparticle diffusion and adsorption of arsenate onto granular ferric hydroxide (GFH), *Water Res.* 38 (2004) 4002-4012.

[75] D. Vasudevan, T.A. Arey, D.R. Dickstein, M.H. Newman, T.Y. Zhang, H.M. Kinnear, M.M. Bader, Nonlinearity of cationic aromatic amine sorption to aluminosilicates and soils: role of intermolecular cation-pi interactions, *Environ. Sci. Technol.* 47 (2013) 14119-14127.

[76] M. Pena, X. Meng, G.P. Korfiatis, C. Jing, Adsorption mechanism of arsenic on nanocrystalline titanium dioxide, *Environ. Sci. Technol.* 40 (2006) 1257-1262.

[77] S. Zhang, X.Y. Li, J.P. Chen, An XPS study for mechanisms of arsenate adsorption onto a magnetite-doped activated carbon fiber, *J. Colloid. Interf. Sci.* 343 (2010) 232-238.

[78] Y. Arai, E.J. Elzinga, D.L. Sparks, X-ray absorption spectroscopic investigation of arsenite and arsenate adsorption at the aluminum oxide-water interface, *J. Colloid. Interf. Sci.* 235 (2001) 80-88.

[79] J.J. Pignatello, B. Xing, Mechanisms of slow sorption of organic chemicals to natural particles, *Environ. Sci. Technol.* 30 (1995) 1-11.

[80] L. Cumbal, A.K. SenGupta, Arsenic removal using polymer-supported hydrated iron (III) oxide nanoparticles: role of donnan membrane effect, *Environ. Sci. Technol.* 39 (2005) 6508-6515.

[81] B. Chen, Z. Zhu, Y. Guo, Y. Qiu, J. Zhao, Facile synthesis of mesoporous Ce-Fe bimetal

oxide and its enhanced adsorption of arsenate from aqueous solutions, *J. Colloid Interf. Sci.* 398 (2013) 142-151.

[82] H. Furukawa, K.E. Cordova, M. O'Keeffe, O.M. Yaghi, The chemistry and applications of metal-organic frameworks, *Science* 341 (2013) 1230444.

[83] L.E. Kreno, K. Leong, O.K. Farha, M. Allendorf, R.P. Van Duyne, J.T. Hupp, Metal-organic framework materials as chemical sensors, *Chem. Rev.* 112 (2012) 1105-1125.

[84] R. Ozer, J. Hinestroza, One-step growth of isoreticular luminescent metal–organic frameworks on cotton fibers, *RSC Adv.* 5 (2015) 15198-15204.

[85] M.D. Allendorf, C.A. Bauer, R.K. Bhakta, R.J. Houk, Luminescent metal-organic frameworks, *Chem. Soc. Rev.* 38 (2009) 1330-1352.

[86] Y. Cui, B. Chen, G. Qian, Lanthanide metal-organic frameworks for luminescent sensing and light-emitting applications, *Coord. Chem. Rev.* 273-274 (2014) 76-86.

[87] W. Zhang, J. Yu, Y. Cui, X. Rao, Y. Yang, G. Qian, Assembly and tunable luminescence of lanthanide-organic frameworks constructed from 4-(3,5-dicarboxyphenyl)pyridine-2,6-dicarboxylate ligand, *J. Alloys Compd.* 551 (2013) 616-620.

[88] J.J. Qian, L.G. Qiu, Y.M. Wang, Y.P. Yuan, A.J. Xie, Y.H. Shen, Fabrication of magnetically separable fluorescent terbium-based MOF nanospheres for highly selective trace-level detection of TNT, *Dalton. Trans.* 43 (2014) 3978-3983.

[89] A. Lan, K. Li, H. Wu, D.H. Olson, T.J. Emge, W. Ki, M. Hong, J. Li, A luminescent microporous metal-organic framework for the fast and reversible detection of high explosives, *Angew. Chem. Int. Ed.* 48 (2009) 2334-2338.

[90] S. Khanjani, A. Morsali, Layer by layer growth of nano porous lead(ii) coordination polymer on natural silk fibers and its application in removal and recovery of iodide, *Cryst. Eng. Comm.* 14 (2012) 8137-8142.

[91] N.L. Rosi, J. Kim, M. Eddaoudi, B. Chen, M. O'Keeffe, O.M. Yaghi, Rod packings and metal-organic frameworks constructed from rod-shaped secondary building units, *J. Am. Chem. Soc.* 127 (2005) 1504-1518.

[92] B. Chen, L. Wang, F. Zapata, G. Qian, E.B. Lobkovsky, A luminescent microporous metal-

organic framework for the recognition and sensing of anions, *J. Am. Chem. Soc.* 130 (2008) 6718-6719.

[93] W. Yang, Z.Q. Bai, W.Q. Shi, L.Y. Yuan, T. Tian, Z.F. Chai, H. Wang, Z.M. Sun, MOF-76: from a luminescent probe to highly efficient U(VI) sorption material, *Chem. Commun.* 49 (2013) 10415-10417.

[94] X. Lian, B. Yan, A lanthanide metal–organic framework (MOF-76) for adsorbing dyes and fluorescence detecting aromatic pollutants, *RSC Adv.* 6 (2016) 11570-11576.

[95] W. Yang, J. Feng, S. Song, H. Zhang, Microwave-assisted modular fabrication of nanoscale luminescent metal-organic framework for molecular sensing, *ChemPhysChem* 13 (2012) 2734-2738.

[96] Y. Xiao, L. Wang, Y. Cui, B. Chen, F. Zapata, G. Qian, Molecular sensing with lanthanide luminescence in a 3D porous metal-organic framework, *J. Alloys Compd.* 484 (2009) 601-604.

[97] W. Wang, Y. Li, M. Sun, C. Zhou, Y. Zhang, Y. Li, Q. Yang, Colorimetric and fluorescent nanofibrous film as a chemosensor for Hg^{2+} in aqueous solution prepared by electrospinning and host–guest interaction, *Chem. Commun.* 48 (2012) 6040-6042.

[98] W. Wang, X. Wang, Q. Yang, X. Fei, M. Sun, Y. Song, A reusable nanofibrous film chemosensor for highly selective and sensitive optical signaling of Cu^{2+} in aqueous media, *Chem. Commun.* 49 (2013) 4833-4835.

[99] W. Wang, Q. Yang, L. Sun, H. Wang, C. Zhang, X. Fei, M. Sun, Y. Li, Preparation of fluorescent nanofibrous film as a sensing material and adsorbent for Cu^{2+} in aqueous solution via copolymerization and electrospinning, *J. Hazard. Mater.* 194 (2011) 185-192.

[100] Y. Zhang, S. Yuan, G. Day, X. Wang, X. Yang, H.-C. Zhou, Luminescent sensors based on metal-organic frameworks, *Coordin. Chem. Rev.* 354 (2018) 28-45.

[101] D. Zacher, O. Shekhah, C. Wöll, R.A. Fischer, Thin films of metal-organic frameworks, *Chem. Soc. Rev.* 38 (2009) 1418-1429.

[102] R.M. Abdelhameed, O.M. Kamel, A. Amr, J. Rocha, A.M. Silva, Anti-mosquito activity of a titanium-organic framework supported on fabrics, *ACS Appl. Mater. Inter.* 9 (2017)

22112-22120.

[103] M.J. Neufeld, A. Lutzke, J.B. Tapia, M.M. Reynolds, Metal-organic framework/chitosan hybrid materials promote nitric oxide release from S-nitrosoglutathione in aqueous solution, *ACS Appl. Mater. Inter.* 9 (2017) 5139-5148.

[104] M.J. Neufeld, B.R. Ware, A. Lutzke, S.R. Khetani, M.M. Reynolds, Water-stable metal-organic framework/polymer composites compatible with human hepatocytes, *ACS Appl. Mater. Inter.* 8 (2016) 19343-19352.

[105] M. Meilikhov, K. Yusenko, E. Schollmeyer, C. Mayer, H.J. Buschmann, R.A. Fischer, Stepwise deposition of metal organic frameworks on flexible synthetic polymer surfaces, *Dalton. Trans.* 40 (2011) 4838-4841.

[106] P. Küsgens, S. Siegle, S. Kaskel, Crystal Growth of the metal-organic framework $Cu_3(BTC)_2$ on the surface of pulp fibers, *Adv. Eng. Mater.* 11 (2009) 93-95.

[107] X. Xiao, X. Liu, F. Chen, D. Fang, C. Zhang, L. Xia, W. Xu, Highly anti-UV properties of silk fiber with uniform and conformal nanoscale TiO_2 coatings via atomic layer deposition, *ACS Appl. Mater. Inter.* 7 (2015) 21326-21333.

[108] J. Nam, Y.H. Park, Morphology of regenerated silk fibroin: effects of freezing temperature, alcohol addition, and molecular weight, *J. Appl. Polym. Sci.* 81 (2001) 3008-3021.

[109] J. Pérez-Rigueiro, M. Elices, J. Llorca, C. Viney, Effect of degumming on the tensile properties of silkworm (Bombyx mori) silk fiber, *J. Appl. Polym. Sci.* 84 (2002) 1431-1437.

[110] A.R. Abbasi, K. Akhbari, A. Morsali, Dense coating of surface mounted CuBTC metal-organic framework nanostructures on silk fibers, prepared by layer-by-layer method under ultrasound irradiation with antibacterial activity, *Ultrason. Sonochem.* 19 (2012) 846-852.

[111] A.R. Abbasi, J.a.-D. Aali, A. Azadbakht, A. Morsali, V. Safarifard, Synthesis and characterization of TMU-16-NH_2 metal-organic framework nanostructure upon silk fiber: study of structure effect on morphine and methyl orange adsorption affinity, *Fiber. Polym.* 16 (2015) 1193-1200.

[112] O. Shekhah, H. Wang, S. Kowarik, F. Schreiber, M. Paulus, M. Tolan, C. Sternemann, F. Evers, D. Zacher, R.A. Fischer, Step-by-step route for the synthesis of metal-organic frameworks, *J. Am. Chem. Soc.* 129 (2007) 15118-15119.

[113] M.R. Awual, A novel facial composite adsorbent for enhanced copper(II) detection and removal from wastewater, *Chem. Eng. J.* 266 (2015) 368-375.

[114] M.R. Awual, T. Yaita, S.A. El-Safty, H. Shiwaku, S. Suzuki, Y. Okamoto, Copper(II) ions capturing from water using ligand modified a new type mesoporous adsorbent, *Chem. Eng. J.* 221 (2013) 322-330.

[115] J. Yao, K. Zhang, H. Zhu, F. Ma, M. Sun, H. Yu, J. Sun, S. Wang, Efficient ratiometric fluorescence probe based on dual-emission quantum dots hybrid for on-site determination of copper ions, *Anal. Chem.* 85 (2013) 6461-6468.

[116] C. Liu, B. Yan, A novel photofunctional hybrid material of pyrene functionalized metal-organic framework with conformation change for fluorescence sensing of Cu^{2+}, *Sensor. Actuat. B-Chem.* 235 (2016) 541-546.

[117] W. Lamoolphak, W. De-Eknamkul, A. Shotipruk, Hydrothermal production and characterization of protein and amino acids from silk waste, *Bioresour. Technol.* 99 (2008) 7678-7685.

[118] B. Mortimer, J. Guan, C. Holland, D. Porter, F. Vollrath, Linking naturally and unnaturally spun silks through the forced reeling of bombyx mori, *Acta. Biomater.* 11 (2015) 247-255.

[119] G. Wu, P. Song, D. Zhang, Z. Liu, L. Li, H. Huang, H. Zhao, N. Wang, Y. Zhu, Robust composite silk fibers pulled out of silkworms directly fed with nanoparticles, *Int. J. Biol. Macromol.* 104 (2017) 533-538.

[120] N.L. Rosi, J. Kim, M. Eddaoudi, B. Chen, M. O'Keeffe, O.M. Yaghi, Rod packings and metal-organic frameworks constructed from rod-shaped secondary building units, *J. Am. Chem. Soc.* 127 (2005) 1504-1518.

[121] J. Zhao, B. Gong, W.T. Nunn, P.C. Lemaire, E.C. Stevens, F.I. Sidi, P.S. Williams, C.J. Oldham, H.J. Walls, S.D. Shepherd, M.A. Browe, G.W. Peterson, M.D. Losego, G.N.

Parsons, Conformal and highly adsorptive metal-organic framework thin films via layer-by-layer growth on ALD-coated fiber mats, *J. Mater. Chem. A* 3 (2015) 1458-1464.

[122] C.-Z. Zhou, F. Confalonieri, N. Medina, Y. Zivanovic, C. Esnault, T. Yang, M. Jacquet, J. Janin, M. Duguet, R. Perasso, Fine organization of Bombyx mori fibroin heavy chain gene, *Nucleic Acids Res.* 28 (2000) 2413-2419.

[123] Y. Shen, M.A. Johnson, D.C. Martin, Microstructural characterization of Bombyx mori silk fibers, *Macromol.* 31 (1998) 8857-8864.

[124] M.J. Neufeld, J.L. Harding, M.M. Reynolds, Immobilization of metal-organic framework copper(II) benzene-1,3,5-tricarboxylate (CuBTC) onto cotton fabric as a nitric oxide release catalyst, *ACS Appl. Mater. Inter.* 7 (2015) 26742-26750.

[125] M. Liu, G. Li, Z. Cheng, A novel dual-functional fluorescent chemosensor for the selective detection of 2,4,6-trinitrotoluene and Hg^{2+}, *New J. Chem.* 39 (2015) 8484-8491.

[126] M. Almáši, V. Zeleňák, J. Kuchár, S. Bourrelly, P.L. Llewellyn, New members of MOF-76 family containing Ho(III) and Tm(III) ions: Characterization, stability and gas adsorption properties, *Colloid. Surface. A* 496 (2016) 114-124.

[127] J. Ethiraj, F. Bonino, J.G. Vitillo, K.A. Lomachenko, C. Lamberti, H. Reinsch, K.P. Lillerud, S. Bordiga, Solvent-driven gate opening in MOF-76-Ce: effect on CO_2 adsorption, *ChemSusChem* 9 (2016) 713-719.

[128] A.R. Abbasi, K. Akhbari, A. Morsali, Dense coating of surface mounted CuBTC metal–organic framework nanostructures on silk fibers, prepared by layer-by-layer method under ultrasound irradiation with antibacterial activity, *Ultrason. Sonochem.* 19 (2012) 846-852.

[129] N.A. Khan, S.H. Jhung, Synthesis of metal-organic frameworks (MOFs) with microwave or ultrasound: rapid reaction, phase-selectivity, and size reduction, *Coordin. Chem. Rev.* 285 (2015) 11-23.

[130] H. Guo, Y. Zhu, S. Qiu, J.A. Lercher, H. Zhang, Coordination modulation induced synthesis of nanoscale Eu(1-x)Tb(x)-metal-organic frameworks for luminescent thin films, *Adv. Mater.* 22 (2010) 4190-4192.

[131] T.-W. Duan, B. Yan, Hybrids based on lanthanide ions activated yttrium metal-organic

frameworks: functional assembly, polymer film preparation and luminescence tuning, *J. Mater. Chem. C* 2 (2014) 5098-5104.

[132] W. Yang, J. Feng, H. Zhang, Facile and rapid fabrication of nanostructured lanthanide coordination polymers as selective luminescent probes in aqueous solution, *J. Mater. Chem.* 22 (2012) 6819.

[133] J. Zhao, Y.N. Wang, W.W. Dong, Y.P. Wu, D.S. Li, Q.C. Zhang, A robust luminescent Tb(III)-MOF with lewis basic pyridyl sites for the highly sensitive detection of metal ions and small molecules, *Inorg. Chem.* 55 (2016) 3265-3271.

[134] Z. Hao, X. Song, M. Zhu, X. Meng, S. Zhao, S. Su, W. Yang, S. Song, H. Zhang, One-dimensional channel-structured Eu-MOF for sensing small organic molecules and Cu^{2+} ion, *J. Mater. Chem. A* 1 (2013) 11043-11050.

[135] B. Liu, W.P. Wu, L. Hou, Y.Y. Wang, Four uncommon nanocage-based Ln-MOFs: highly selective luminescent sensing for Cu^{2+} ions and selective CO_2 capture, *Chem. Commun.* 50 (2014) 8731-8734.

[136] L. Chu, J. Wang, J. Dong, H. Liu, X. Sun, Treatment of coking wastewater by an advanced fenton oxidation process using iron powder and hydrogen peroxide, *Chemosphere* 86 (2012) 409-414.

[137] S. Jia, H. Han, H. Zhuang, P. Xu, B. Hou, Advanced treatment of biologically pretreated coal gasification wastewater by a novel integration of catalytic ultrasound oxidation and membrane bioreactor, *Bioresour. Technol.* 189 (2015) 426-429.

[138] S. Jia, H. Han, B. Hou, H. Zhuang, Advanced treatment of biologically pretreated coal gasification wastewater by a novel integration of three-dimensional catalytic electro-Fenton and membrane bioreactor, *Bioresour. Technol.* 198 (2015) 918-921.

[139] P. Xu, H. Han, H. Zhuang, B. Hou, S. Jia, C. Xu, D. Wang, Advanced treatment of biologically pretreated coal gasification wastewater by a novel integration of heterogeneous fenton oxidation and biological process, *Bioresour. Technol.* 182 (2015) 389-392.

[140] M.S. Diallo, S. Christie, P. Swaminathan, J.H. Johnson, W.A. Goddard, Dendrimer

enhanced ultrafiltration. 1. Recovery of Cu(II) from aqueous solutions using PAMAM dendrimers with ethylene diamine core and terminal NH$_2$ groups, *Environ. Sci. Technol.* 39 (2005) 1366-1377.

[141] R.R. Dash, C. Balomajumder, A. Kumar, Removal of cyanide from water and wastewater using granular activated carbon, *Chem. Eng. J.* 146 (2009) 408-413.

[142] P.A. Moussas, A.I. Zouboulis, Synthesis, characterization and coagulation behavior of a composite coagulation reagent by the combination of polyferric sulfate (PFS) and cationic polyelectrolyte, *Sep. Purif. Technol.* 96 (2012) 263-273.

[143] C. Na, Y. Zhang, M. Deng, X. Quan, S. Chen, Y. Zhang, Evaluation of the detoxication efficiencies for acrylonitrile wastewater treated by a combined anaerobic oxic-aerobic biological fluidized tank (A/O-ABFT) process: Acute toxicity and zebrafish embryo toxicity, *Chemosphere* 154 (2016) 1-7.

[144] M. Dehua, L. Cong, Z. Xiaobiao, L. Rui, C. Lujun, Acute toxicity and chemical evaluation of coking wastewater under biological and advanced physicochemical treatment processes, *Environ. Sci. Pollut. Res.* 23 (2016) 18343-18352.

[145] Y.M. Li, G.W. Gu, J.F. Zhao, H.Q. Yu, Y.L. Qiu, Y.Z. Peng, Treatment of coke-plant wastewater by biofilm systems for removal of organic compounds and nitrogen, *Chemosphere* 52 (2003) 997-1005.

[146] M. Czaplicka, Qualitative and quantitative determination of halogenated derivatives in wastewater from coking plant, *J. Sep. Sci.* 26 (2003) 1067-1071.

Acknowledgement

I would like to extend my sincere gratitude to all those who helped me during the writing of this thesis.

First of all, I would like to express my gratitude to my supervisor, Prof. Zhongfang Lei, for her instructive advice on my thesis and encouragement throughout my research work. I could not have completed my thesis without her enlightening instructions and patient guidance.

I am also deeply indebted to my co-supervisors, Prof. Zhenya Zhang and Prof. Yasuhisa Adachi, for their direct and indirect help to me.

Special thanks should go to Prof. Zhongfang Lei, Prof. Zhenya Zhang, Prof. Kazuya Shimizu, and Prof. Helmut Yabar for being the thesis committee members and their valuable and useful comments on my thesis.

I also owe my sincere gratitude to my friends and my fellow classmates who helped me a lot for my study and living in Tsukuba.

Furthermore, I would like to thank the financial support by the Chinese Scholarship Committee (CSC) scholarship (201606260184) for my PhD study abroad.

I should finally like to express my gratitude to my beloved parents and my wife who have always been helping me out of difficulties and supporting without any word of complaint.

Publications

1. **<u>Jie Li</u>**, Yi-nan Wu, Zehua Li, Miao Zhu, Fengting Li. Characteristics of arsenate removal from water by metal-organic frameworks (MOFs). *Water Science & Technology*, 2014, 70, 1391-1397.

2. **<u>Jie Li</u>**, Yi-nan Wu, Zehua Li, Bingru Zhang, Miao Zhu, Xiao Hu, Yiming Zhang, Fengting Li. Zeolitic imidazolate framework-8 with high efficiency in trace arsenate adsorption and removal from water. *Journal of Physical Chemistry C*, 2014, 118, 27382-27387.

3. **<u>Jie Li</u>**, Xiao Yuan, Huangpu Zhao, Fengting Li, Zhongfang Lei, Zhenya Zhang. Highly efficient one-step advanced treatment of biologically pretreated coking wastewater by an integration of coagulation and adsorption process. *Bioresource Technology*, 2018, 247, 1206-1209.

4. **<u>Jie Li</u>**, Xiao Yuan, Yi-nan Wu, Xiaoliang Ma, Fengting Li, Bingru Zhang, Ying Wang, Zhongfang Lei, Zhenya Zhanga. From powder to cloth: facile fabrication of dense MOF-76(Tb) coating onto natural silk fiber for feasible detection of copper ions. *Chemical Engineering Journal*, 2018, 350, 637-644.

5. **<u>Jie Li</u>**, Yi-nan Wu, Fengting Li, Zhongfang Lei, Zhenya Zhang. Full-scale performance of hybrid AS/PDDA coagulant for steady removal of turbidity and color from raw water with high turbidity and violent quality fluctuation. (under preparation)

6. **<u>Jie Li</u>**, Chaofan Yu, Yingjing Zhu, Jinjin Xu, Ying Wang, Fengting Li. Comparison and optimization of intrinsic peroxidase-like catalytic activity within iron-based MOFs material for convenient detection of trace antibiotics in water. (under preparation)